BLDC Motor Modelling and Control – A Matlab®/Simulink® Implementation

– Master Thesis work by Stefán Baldursson –

May, 2005

Institutionen för Energi och Miljö
International masters program in Electric Power Engineering
CHALMERS TEKNISKA HÖGSKOLA
Göteborg, Sverige, 2005
Examinator: Torbjörn Thiringer

Abstract

This thesis presents a model of a three phase star-connected brushless direct current (bldc) motor. The construction and operation of both conventional dc motors and bldc motors is presented and state-space models are derived for each. Matlab®/Simulink® models are developed for each motor type and their validity is verified. Torque-, speed- and position control is applied using hysteresis band control, pwm control, and variable dc-link voltage control. The different control strategies are tested on the bldc motor and their performance evaluated. The frequency content of the dc-link current is investigated for each control method and the impact of commutation delay and switching losses is discussed. Simulations show that all the control strategies work quite well although each method has its drawbacks. The frequency spectrum of the dc-link current shows that hysteresis band control may not be suitable where load variations are large. The variable dc-link voltage method turns out to be the best solution in applications where torque ripples and switching losses must me minimized. Commutation delay is necessary in practice, but the simulations show that it should be kept as short as possible because it causes increased torque ripples.

Keywords: Brushless motors, bldc, modelling, control.

Acknowledgements

I would like to thank my supervisor Dr. Torbjörn Thiringer at Chalmers University for excellent help and patience.

Contents

List of Figures vi

List of Tables ix

List of Symbols, Subscripts and Abbreviations ix

1 Introduction 1

2 DC Motors 3
2.1 Construction . . . 3
2.2 Operation . . . 4
2.3 Mathematical Model . . . 6

3 BLDC Motors 8
3.1 Construction . . . 8
3.2 Operation . . . 9
3.3 Mathematical Model . . . 12

4 Matlab®/Simulink® Models 14
4.1 The DC Motor . . . 14
4.1.1 The model . . . 14
4.1.2 Simulation . . . 15
4.2 The BLDC motor . . . 18
4.2.1 The motor . . . 18
4.2.2 The Inverter . . . 20
4.2.3 Simulation . . . 28

5 Control 32
5.1 Hysteresis Band Control . . . 32
5.1.1 Torque Control . . . 33
5.1.2 Speed Control . . . 36
5.2 PWM Control . . . 39

5.2.1 Torque Control 39
5.2.2 Speed Control 42
5.2.3 Position Control 49
5.3 Variable DC-Link Voltage Control 51
5.3.1 Torque Control 51
5.3.2 Speed Control 54
5.3.3 Position Control 61
5.4 Frequency Analysis 63
5.4.1 Uncontrolled motor 63
5.4.2 Hysteresis control 65
5.4.3 PWM 66
5.4.4 Variable DC-Link Voltage 66

6 Turn-ON Delay and Losses **68**
6.1 Turn-ON Delay 68
6.2 ON-state Losses 70

7 Conclusions **72**
7.1 Summary 72
7.2 Further Work 73

Bibliography **74**

List of Figures

2.1 Cross section of a two pole dc motor 3
2.2 Brushes and commutator segments of the dc motor 4
2.3 DC-motor operated with a variable dc voltage 5
2.4 DC-motor operated with a step-down chopper 5
2.5 Turn-on signal and current waveforms in a step-down chopper 5
2.6 DC-motor equivalent circuit 6

3.1 BLDC motor transverse section 9
3.2 Ideal back-emf's, phase currents, and position sensor signals . 10
3.3 BLDC motor cross section and phase energizing sequence . . . 11
3.4 Simplified bldc drive scheme 11

4.1 The dc motor model 14
4.2 DC motor speed 16
4.3 Electrical torque of the dc motor 16
4.4 Torque-speed plot of the dc motor 17
4.5 DC-link current 17
4.6 The bldc drive model 18
4.7 Contents of the bldc motor block 19
4.8 Calculation of trapezoidal waveforms and position signals . . . 19
4.9 Torque calculation in Subsystem1 20
4.10 Circuit configuration in each 60° 21
4.11 The two circuit topologies from figure 4.10 21
4.12 Circuit configuration during hard chopping 24
4.13 The two circuit topologies from figure 4.12 25
4.14 Circuit configuration during soft chopping 26
4.15 The two circuit topologies from figure 4.14 27
4.16 Rotor speed 28
4.17 Electrical torque 29
4.18 Zoomed view of the electrical torque 29
4.19 Torque-speed plot 30
4.20 Phase currents 30

4.21 Zoomed view of phase currents (solid) and back-emf's (dashed) 31

5.1 Hysteresis torque control system 33
5.2 Electrical torque in hysteresis torque control exposed to a load-step 34
5.3 Rotor speed in hysteresis torque control exposed to a loadstep 35
5.4 Phase currents in hysteresis torque control exposed to a loadstep 35
5.5 Hysteresis speed control system 36
5.6 Rotor speed in hysteresis speed control exposed to a loadstep . 37
5.7 Electrial torque in hysteresis speed control exposed to a loadstep 37
5.8 Phase currents in hysteresis speed control exposed to a loadstep 38
5.9 PWM torque control system 39
5.10 Electrical torque in pwm torque control exposed to a loadstep 40
5.11 Rotor speed in pwm torque control exposed to a loadstep . . . 41
5.12 Phase currents in pwm torque control exposed to a loadstep . 41
5.13 PWM speed control system 42
5.14 Rotor speed in pwm speed control at no load ($\alpha_\omega = \alpha_e$) 43
5.15 Electrical torque in pwm speed control at no load ($\alpha_\omega = \alpha_e$) . 43
5.16 Phase currents in pwm speed control at no load ($\alpha_\omega = \alpha_e$) . . 44
5.17 Rotor speed in pwm speed control at no load ($\alpha_\omega = 0.01\alpha_e$) . . 45
5.18 Electrial torque in pwm speed control at no load ($\alpha_\omega = 0.01\alpha_e$) 45
5.19 Phase currents in pwm speed control at no load ($\alpha_\omega = 0.01\alpha_e$) 46
5.20 Rotor speed in pwm speed control at no load ($\alpha_\omega = 0.1\alpha_e$) . . 46
5.21 Electrical torque in pwm speed control at no load ($\alpha_\omega = 0.1\alpha_e$) 47
5.22 Phase currents in pwm speed control at no load ($\alpha_\omega = 0.1\alpha_e$) . 47
5.23 Rotor speed in pwm speed control at maximum load step ($\alpha_\omega = 0.1\alpha_e$) 48
5.24 PWM position control system 49
5.25 Rotor angle in pwm position control at no load 50
5.26 Rotor angle in pwm position control at maximum load 50
5.27 Varible dc-link voltage torque control system 51
5.28 Electrical torque in variable dc-link voltage torque control . . 52
5.29 Rotor speed in variable dc-link voltage torque control 52
5.30 Phase currents in variable dc-link voltage torque control . . . 53
5.31 Varible dc-link voltage, speed control system 54
5.32 Rotor speed in variable dc-link voltage speed control control at no load ($\alpha_\omega = \alpha_e$) 55
5.33 Electrical torque in variable dc-link voltage speed control at no load ($\alpha_\omega = \alpha_e$) 55
5.34 Phase currents in variable dc-link voltage speed control at no load ($\alpha_\omega = \alpha_e$) 56

5.35 Rotor speed in variable dc-link voltage speed control at no load ($\alpha_\omega = 0.01\alpha_e$) 56
5.36 Electrical torque in variable dc-link voltage speed control at no load ($\alpha_\omega = 0.01\alpha_e$) 57
5.37 Phase currents in variable dc-link voltage speed control at no load ($\alpha_\omega = 0.01\alpha_e$) 57
5.38 Rotor speed in variable dc-link voltage speed control at no load ($\alpha_\omega = 0.1\alpha_e$) 58
5.39 Electrical torque in variable dc-link voltage speed control at no load ($\alpha_\omega = 0.1\alpha_e$) 58
5.40 Phase currents in variable dc-link voltage speed control at no load ($\alpha_\omega = 0.1\alpha_e$) 59
5.41 Rotor speed in variable dc-link voltage speed control at maximum load step ($\alpha_\omega = 0.1\alpha_e$) 59
5.42 Electrical torque in variable dc-link voltage speed control at maximum load step ($\alpha_\omega = 0.1\alpha_e$) 60
5.43 Varible dc-link voltage position control system 61
5.44 Rotor angle in variable dc-link voltage position control at no load 61
5.45 Rotor angle in variable dc-link voltage position control at maximum load 62
5.46 Zoomed view of the electrical torque at no load speed 63
5.47 Zoomed view of the electrical torque at maximum load 64
5.48 Power spectrum of the dc-link current at no-load speed 64
5.49 Power spectrum of the dc-link current in hysteresis speed control at no load 65
5.50 Power spectrum of the dc-link current in hysteresis speed control at maximum load 66
5.51 Power spectrum of the dc-link current in pwm speed control at no load 67
5.52 Power spectrum of the dc-link current in pwm speed control at maximum load 67

6.1 Phase currents. A 1 ms turn-on delay is applied at 0.03 s . . . 69
6.2 Electrial torque. 1 ms turn-on delay is applied at 0.03 s 69
6.3 Rotor speed when on-state resistance of switches is 2 Ω 70
6.4 Electrical torque when on-state resistance of switches is 2 Ω . 71
6.5 Power dissipation in switches when on-state resistance is 2 Ω . 71

List of Tables

3.1 Switching sequence 11

4.1 BLDC motor parameters 15
4.2 Inverter output voltages 23
4.3 BLDC motor input voltages during hard chopping 25
4.4 BLDC motor input voltages during soft chopping 27

List of Symbols, subscripts and abbreviations

Symbols

α	$\frac{\ln 9}{t_{re}}$ (except firing angle in fig. 2.3)
A	phase A
B	phase B
C	phase C
e	back-emf
D	diode
F	trapezoidal function
H	position sensor signal
i	current
J	inertia
k	constant
L	phase inductance
n	rotor speed (rpm)
N	north magnetic pole
Q	electronic switch
R	phase resistance
S	south magnetic pole
t	time
t_{re}	rise time of current
T	torque
u	phase-to-phase voltage minus phase-to-phase back-emf
v	phase-to-phase voltage
V	dc voltage
Z	phase impedance
θ	angle
ω	angular speed

Subscripts

ab	phase a to phase b
bc	phase b to phase c
ca	phase c to phase a
com	commutation
d	diode
e	electrical
E	back-emf
f	friction
i	integral
L	load
m	mechanical
p	proportional
ref	reference value
s	source
t	torque

Abbreviations

bldc	brushless dc
dc	direct current
emf	electromotive force
pwm	pulse width modulation
rpm	revolutions per minute

Chapter 1

Introduction

Conventional dc motors have many attractive properties such as high efficiency and linear torque-speed characteristics. The control of dc motors is also simple and does not require complex hardware. However, the main drawback of the dc motor is the need of periodic maintenance. The brushes of the mechanical commutator eventually wear out and need to be replaced. The mechanical commutator has other undesirable effects such as sparks, acoustic noise and carbon particles coming from the brushes. Brushless dc (bldc) motors can in many cases replace conventional dc motors. Such motor replacement is studied in [1]. Despite the name, bldc motors are actually a type of permanent magnet synchronous motors. They are driven by dc voltage but current commutation is done by solid state switches. The commutation instants are determined by the rotor position and the position of the rotor is detected either by position sensors or by sensorless techniques. Bldc motors have many advantages over conventional dc motors. A few of these are [2]:

- Long operating life
- High dynamic response
- High efficiency
- Better speed vs. torque characteristics
- Noiseless operation
- Higher speed range
- Higher torque-weight ratio

BLDC motors are available in many different power ratings, from very small motors as used in hard disk drives to larger motors used in electric vehicles. Three-phase motors are most common but two-phase motors are also found in many applications.

The purpose of this report is to build a simple, accurate and fast running Matlab®/Simulink® model of a three phase star-connected bldc motor and compare the function of different control strategies. A simple approach to current sensing and pwm current control of bldc motors has been presented in [3]. This method will be applied here using hysteresis band control, pwm control and variable dc-link voltage control. Similar, but less extensive, work has been done in [4] where a pwm torque controller was implemented. The model presented here, takes that work one step further with the control of torque, speed and position, using the three control strategies mentioned above. Switching losses and the effects of commutation delay on torque ripples are also treated.

Chapter 2 presents the construction and operation of a conventional dc motor and derives a simple mathematical representation of it.

Chapter 3 presents the bldc motor, its construcion and operation and derives a mathematical model to be used in a Matlab®/Simulink® implementation.

Chapter 4 presents a detailed description of the Matlab®/Simulink® models. The models are tested and their characteristics presented.

Chapter 5 introduces hysteresis band control, pwm control and variable dc-link voltage control. These methods are used in torque-, speed-, and position control of the bldc motor. The control methods are evaluated both in time domain and frequency domain.

Chapter 6 presents the effect of losses in the voltage source and in the inverter, and studies the effect of commutation delay.

Chapter 7 contains a summary of the report and discusses possible topics for further work.

Chapter 2

DC Motors

This chapter describes typical construction and operation of a conventional dc motor and derives a mathematical model that can be simulated efficiently in Matlab®/Simulink®.

2.1 Construction

The dc motor has its armature on the rotor as shown in figure 2.1. The stator has salient magnetic poles that are either made of permanent magnets or special field windings. Current is fed to the rotor windings through brushes that are in contact with copper strips located at the end of the rotor. These copper strips, usually called commutator segments, are connected to the rotor windings.

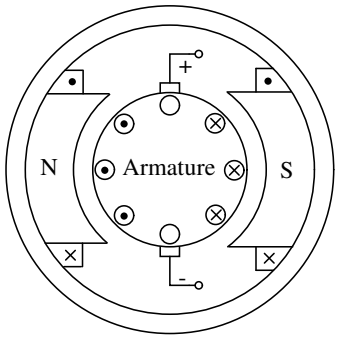

Figure 2.1: Cross section of a two pole dc motor [5]

As the rotor rotates, the brushes move from one segment to another which commutates the current in such a way that the currents in the conductors

under each pole flow in the same direction (from the stator point of view). This is depicted in figures 2.1 and 2.2. The resulting force vectors that act on the rotor windings are all tangential to the rotor periphery and they all contribute to the torque.

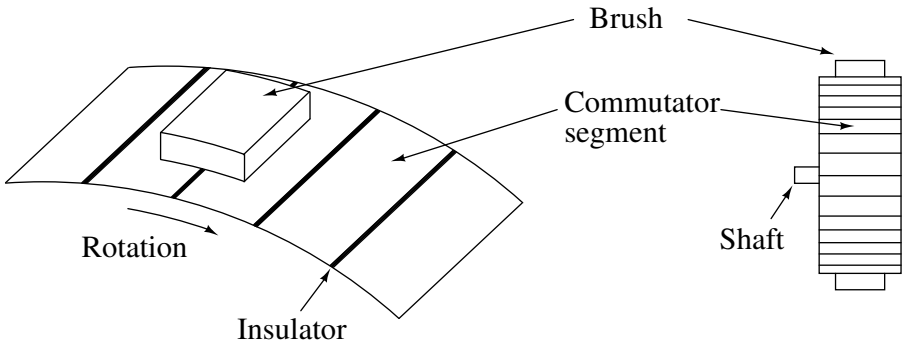

Figure 2.2: Brushes and commutator segments of the dc motor [6]

2.2 Operation

As the name implies, the dc motor is fed from a dc voltage source. The speed can be controlled by varying the applied voltage. This can be achieved by having a variable voltage source or by using a variable resistor connected in series with the armature. The latter method is simple but not very efficient because of the power dissipated in the variable resistor. If the motor is not of the permanent magnet type, the speed can also be varied by changing the field current. Higher efficiency is achieved by using solid state converters such as controlled rectifiers and choppers. Controlled rectifiers are used to create a variable dc voltage. Figure 2.3 shows such arrangement. The voltage is varied by changing the firing angle of the thyristors.

The chopper shown in figure 2.4 consists of an electronic switch that is used to turn the motor on and off at a high rate. When the switch is turned off, the diode provides a path for the inductive armature current. Figure 2.5 shows the turn-on signal and the current waveforms. The current rise and fall lowers the current mean value but it also introduces undesirable current ripple which is transferred to the electric torque. This method is typical for drives in vehicles.

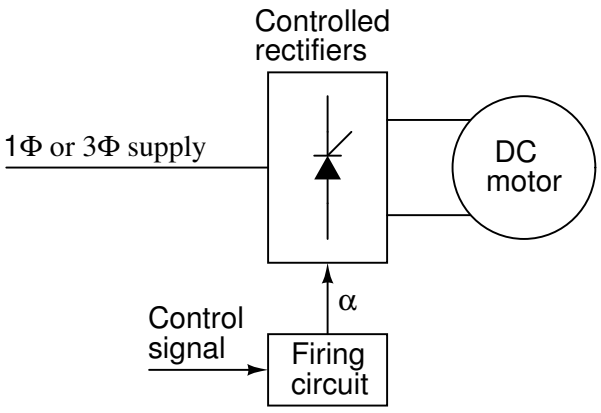

Figure 2.3: DC-motor operated with a variable dc voltage created directly from an ac-grid [5]

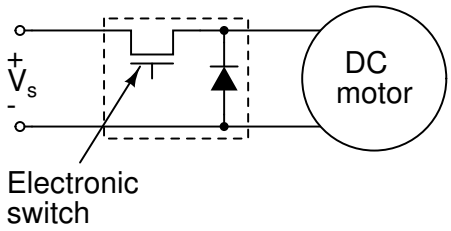

Figure 2.4: DC-motor operated with a step-down chopper [5]

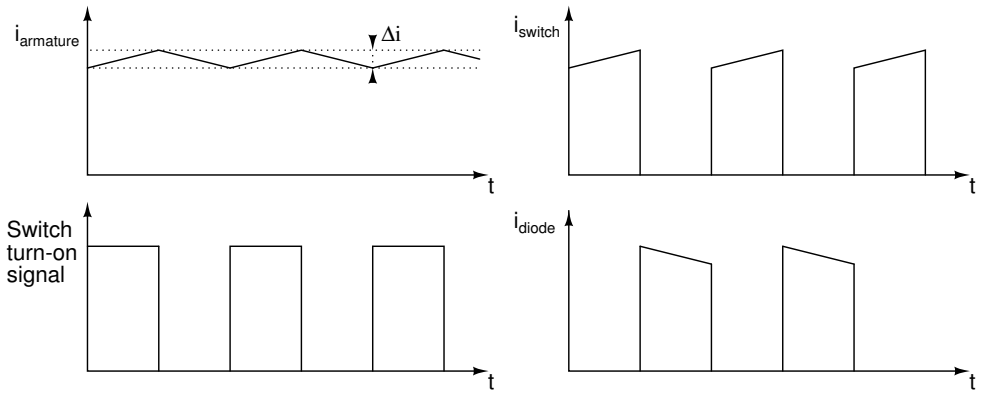

Figure 2.5: Turn-on signal and current waveforms in a step-down chopper [6]

2.3 Mathematical Model

Figure 2.6 shows a simple dc motor circuit model. R and L are the armature resistance and inductance respectively and e is the back-emf. The motor can be described by the following two equations:

$$V_s = Ri + L\frac{di}{dt} + e \tag{2.1}$$

$$T_e = k_f\omega_m + J\frac{d\omega_m}{dt} + T_L. \tag{2.2}$$

Here V_s and i denote the dc-source voltage and the armature current, and T_e, k_f, J and T_L denote the electrical torque, a friction constant, the rotor inertia and a mechanical load.

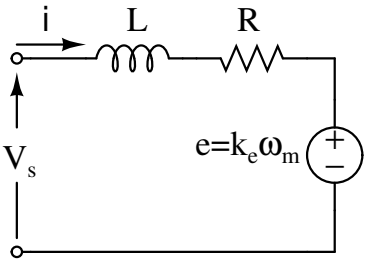

Figure 2.6: DC-motor equivalent circuit [6]

The back-emf and the electrical torque can be written as

$$e = k_e\omega_m \tag{2.3}$$

$$T_e = k_t\omega_m \tag{2.4}$$

where k_e and k_t are the back-emf constant and the torque constant respectively. For modelling purposes it is often convenient to derive a state-space representation of the motor. Equations 2.1 and 2.2 are rewritten as

$$\frac{di}{dt} = -\frac{R}{L}i - \frac{k_e}{L}\omega_m + \frac{1}{L}V_s \tag{2.5}$$

$$\frac{d\omega_m}{dt} = \frac{k_t}{J}i - \frac{k_f}{J}\omega_m - \frac{1}{J}T_L \tag{2.6}$$

and a matrix representation follows directly:

$$\begin{pmatrix} i' \\ \omega_m' \\ \theta_m' \end{pmatrix} = \begin{pmatrix} -\frac{R}{L} & -\frac{k_e}{L} & 0 \\ \frac{k_t}{J} & -\frac{k_f}{J} & 0 \\ 0 & 1 & 0 \end{pmatrix} \begin{pmatrix} i \\ \omega_m \\ \theta_m \end{pmatrix} + \begin{pmatrix} \frac{1}{L} & 0 \\ 0 & -\frac{1}{J} \\ 0 & 0 \end{pmatrix} \begin{pmatrix} V_s \\ T_L \end{pmatrix} \tag{2.7}$$

$$\begin{pmatrix} i \\ \omega_m \\ \theta_m \\ T_e \end{pmatrix} = \begin{pmatrix} 1 & 0 & 0 \\ 0 & 1 & 0 \\ 0 & 0 & 1 \\ k_t & 0 & 0 \end{pmatrix} \begin{pmatrix} i \\ \omega_m \\ \theta_m \end{pmatrix} \tag{2.8}$$

These equations will be used in the Matlab®/Simulink® model presented in chapter 4.

Chapter 3

BLDC Motors

This chapter describes typical construction and operation of a bldc motor and derives a mathematical model that can be simulated efficiently in Matlab®/Simulink®.

3.1 Construction

A bldc motor is a permanent magnet synchronous motor that uses position detectors and an inverter to control the armature currents. The bldc motor is sometimes referred to as an inside-out dc motor because its armature is in the stator and the magnets are on the rotor and its operating characteristics resemble those of a dc motor [5]. Instead of using a mechanical commutator as in the conventional dc motor, the bldc motor employs electronic commutation which makes it a virtually maintenance-free motor.

There are two main types of bldc motors: trapezoidal type and sinusoidal type. In the trapezoidal motor the back-emf induced in the stator windings has a trapezoidal shape and its phases must be supplied with quasi-square currents for ripple-free torque operation. The sinusoidal motor on the other hand has a sinusoidally shaped back-emf and requires sinusoidal phase currents for ripple-free torque operation. The shape of the back-emf is determined by the shape of the rotor magnets and the stator winding distribution.

The sinusoidal motor needs a high resolution position sensor because the rotor position must be known at every time instant for optimal operation. It also requires more complex software and hardware. The trapezoidal motor is a more attractive alternative for most applications due to its simplicity, lower price and higher efficiency [5]. The remaining part of this text discusses trapezoidal bldc motors only.

Bldc motors exist in many different configurations but the three phase

motor is the most common type due to its efficiency and low torque ripple. This type of motor also offers a good compromise between precise control and number of power electronic devices needed to control the stator currents [7]. Figure 3.1 shows a transverse section of a bldc motor. Position detection is usually implemented using three Hall-effect sensors that detect the presence of small magnets that are attached to the motor shaft.

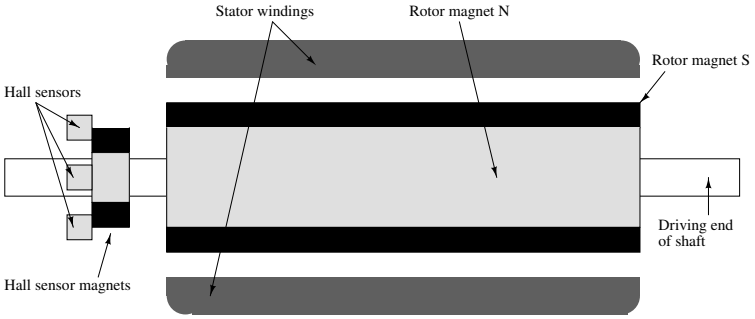

Figure 3.1: BLDC motor transverse section [2]

3.2 Operation

The three phase bldc motor is operated in a two-phases-on fashion, i.e. the two phases that produce the highest torque are energized while the third phase is off. Which two phases are energized depends on the rotor position. The signals from the position sensors produce a three digit number that changes every 60° (electrical degrees) as shown in figure 3.2 (H1, H2, H3). The figure also shows ideal current and back-emf waveforms.

Figure 3.3 shows a cross section of a three-phase star-connected motor along with its phase energizing sequence. Each interval starts with the rotor and stator field lines 120° apart and ends when they are 60° apart. Maximum torque is reached when the field lines are perpendicular. Current commutation is done by a six-step inverter as shown in a simplified form in figure 3.4. The switches are shown as bipolar junction transistors but MOSFET switches are more common. Table 3.1 shows the switching sequence, the current direction and the position sensor signals.

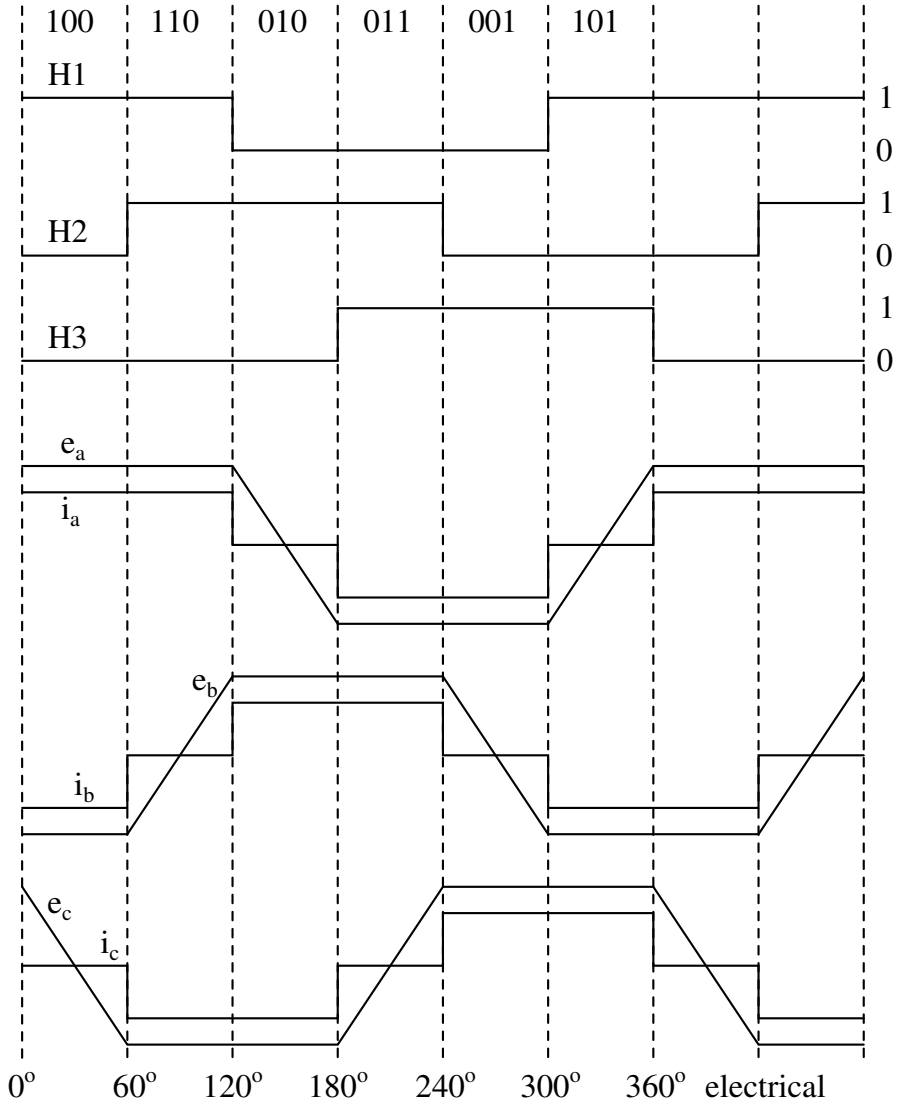

Figure 3.2: Ideal back-emf's, phase currents, and position sensor signals

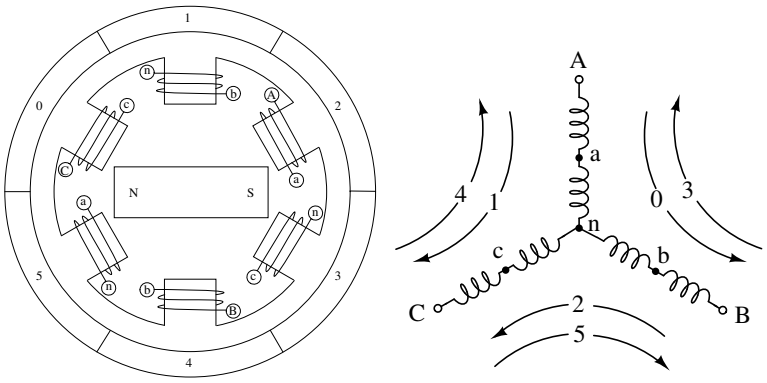

Figure 3.3: BLDC motor cross section and phase energizing sequence [8]

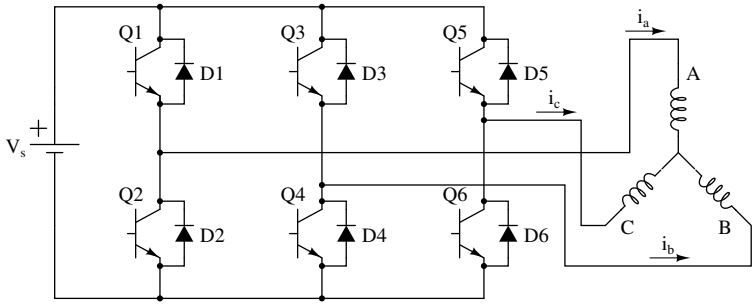

Figure 3.4: Simplified bldc drive scheme

Table 3.1: Switching sequence

Switching interval	Seq. number	Pos. sensors			Switch closed		Phase Current		
		H1	H2	H3			A	B	C
$0° - 60°$	0	1	0	0	Q1	Q4	+	-	off
$60° - 120°$	1	1	1	0	Q1	Q6	+	off	-
$120° - 180°$	2	0	1	0	Q3	Q6	off	+	-
$180° - 240°$	3	0	1	1	Q3	Q2	-	+	off
$240° - 300°$	4	0	0	1	Q5	Q2	-	off	+
$300° - 360°$	5	1	0	1	Q5	Q4	off	-	+

3.3 Mathematical Model

The three phase star connected bldc motor can be described by the following four equations:

$$v_{ab} = R(i_a - i_b) + L\frac{d}{dt}(i_a - i_b) + e_a - e_b \tag{3.1}$$

$$v_{bc} = R(i_b - i_c) + L\frac{d}{dt}(i_b - i_c) + e_b - e_c \tag{3.2}$$

$$v_{ca} = R(i_c - i_a) + L\frac{d}{dt}(i_c - i_a) + e_c - e_a \tag{3.3}$$

$$T_e = k_f\omega_m + J\frac{d\omega_m}{dt} + T_L. \tag{3.4}$$

The symbols v, i and e denote the phase-to-phase voltages, phase currents and phase back-emf's repectively, in the three phases a, b and c. The resistance R and the inductance L are per phase values and T_e and T_L are the electrical torque and the load torque. J is the rotor inertia, k_f is a friction constant and ω_m is the rotor speed. The back-emf's and the electrical torque can be expressed as

$$e_a = \frac{k_e}{2}\omega_m F(\theta_e) \tag{3.5}$$

$$e_b = \frac{k_e}{2}\omega_m F(\theta_e - \frac{2\pi}{3}) \tag{3.6}$$

$$e_c = \frac{k_e}{2}\omega_m F(\theta_e - \frac{4\pi}{3}) \tag{3.7}$$

$$T_e = \frac{k_t}{2}\left[F\Big(\theta_e\Big)i_a + F\Big(\theta_e - \frac{2\pi}{3}\Big)i_b + F\Big(\theta_e - \frac{4\pi}{3}\Big)i_c\right] \tag{3.8}$$

respectively, where k_e and k_t are the back-emf constant and the torque constant. The electrial angle θ_e is equal to the rotor angle times the number of pole pairs ($\theta_e = \frac{p}{2}\theta_m$). The function $F(\cdot)$ gives the trapezoidal waveform of the back-emf. One period of this function can be written as

$$F(\theta_e) = \begin{cases} 1, & 0 \le \theta_e < \frac{2\pi}{3} \\ 1 - \frac{6}{\pi}(\theta_e - \frac{2\pi}{3}) & \frac{2\pi}{3} \le \theta_e < \pi \\ -1 & \pi \le \theta_e < \frac{5\pi}{3} \\ -1 + \frac{6}{\pi}(\theta_e - \frac{5\pi}{3}) & \frac{5\pi}{3} \le \theta_e < 2\pi \end{cases}. \tag{3.9}$$

For a convenient implementation in Matlab®/Simulink®, equations 3.1 - 3.4 must be written in state-space form. These equations need to be modified

to allow a state-space representation. Since each voltage equation is a linear combination of the other two voltage equations only two equations are needed. By throwing away one equation and eliminating one variable using the current relationship

$$i_a + i_b + i_c = 0.$$

the voltage equations become

$$v_{ab} = R(i_a - i_b) + L\frac{d}{dt}(i_a - i_b) + e_a - e_b \tag{3.10}$$

$$v_{bc} = R(i_a + 2i_b) + L\frac{d}{dt}(i_a + 2i_b) + e_b - e_c \tag{3.11}$$

and the complete model is then

$$\begin{pmatrix} i'_a \\ i'_b \\ \omega'_m \\ \theta'_m \end{pmatrix} = \begin{pmatrix} -\frac{R}{L} & 0 & 0 & 0 \\ 0 & -\frac{R}{L} & 0 & 0 \\ 0 & 0 & -\frac{k_f}{J} & 0 \\ 0 & 0 & 1 & 0 \end{pmatrix} \begin{pmatrix} i_a \\ i_b \\ \omega_m \\ \theta_m \end{pmatrix} + \begin{pmatrix} \frac{2}{3L} & \frac{1}{3L} & 0 \\ -\frac{1}{3L} & \frac{1}{3L} & 0 \\ 0 & 0 & \frac{1}{J} \\ 0 & 0 & 0 \end{pmatrix} \begin{pmatrix} v_{ab} - e_{ab} \\ v_{bc} - e_{bc} \\ T_e - T_L \end{pmatrix} \tag{3.12}$$

$$\begin{pmatrix} i_a \\ i_b \\ i_c \\ \omega_m \\ \theta_m \end{pmatrix} = \begin{pmatrix} 1 & 0 & 0 & 0 \\ 0 & 1 & 0 & 0 \\ -1 & -1 & 0 & 0 \\ 0 & 0 & 1 & 0 \\ 0 & 0 & 0 & 1 \end{pmatrix} \begin{pmatrix} i_a \\ i_b \\ \omega_m \\ \theta_m \end{pmatrix} \tag{3.13}$$

Machine models are often transformed to a rotating reference frame for simplification and to improve computational efficiency. This approach is not used here as it has been shown that when the supply voltage is not sinusoidal, such transformation will not improve computational efficiency [9].

Chapter 4

Matlab®/Simulink® Models

This chapter presents the Matlab®/Simulink® implementation of the dc motor and the bldc motor described in chapters 2 and 3. The models have the same parameters that are taken from the datasheet of a commercially available bldc motor. This allows direct comparison of the two models. The bldc motor model is tested and it is verified that it behaves according to the specifications given in the motor's datasheet.

4.1 The DC Motor

4.1.1 The model

The dc motor model shown in figure 4.1 is very simple. The dc motor block contains a state-space block that solves equations 2.7 and 2.8. The input is the dc source voltage V_s and the mechanical load T_L. The outputs are the armature current, rotor speed, rotor angle and the electrical torque.

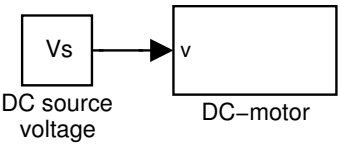

Figure 4.1: The dc motor model

All model constants are defined in the files *constants.m* and *motorpar.m*. *motorpar.m* contains parameters of various bldc motors. Each motor type has a number and a motor is selected by assigning the motor number to the

variable *motortype* in *constants.m*. A simulation is started by running the file *main.m* which runs *constants.m*, starts the simulation and at the end runs the file *plots.m* which plots variables such as current, torque, speed, angle etc.

The available motors are all bldc motors produced by Maxon Precision Motors Inc. The parameters used here are shown in table 4.1 but the complete datasheet is available from Maxon's website [10]. The motor is quite small as it is only 1.2 watts and weighs only 2.8 grams.

Table 4.1: BLDC motor parameters [10]

Motor Data Maxon EC 6 215550		
Number of poles	poles	2
Assigned power rating	W	1.2
Nominal voltage	V	6.0
No load speed	rpm	47130
Stall torque	mNm	0.50
No load current	mA	60
Terminal resistance phase to phase	Ohm	12.50
Terminal inductance phase to phase	mH	0.091
Torque constant	mNm/A	1.05
Rotor inertia	gcm^2	0.005
Friction constant (assumed value)	$\text{Nm} \cdot \text{s}$	$1.38 \cdot 10^{-8}$

4.1.2 Simulation

The simulations are done in Matlab® 6.5 (R13) and Simulink® 5.0 using the default solver ode45. The simulation time is 0.1 seconds and a load torque of 0.23 *mNm* is applied at 0.05 seconds. Figure 4.2 shows the motor speed. A correct value of the no-load speed is achieved by selecting a suitable value of the friction constant k_f. Otherwise, the no-load speed becomes a little too high. Figure 4.3 shows the electrical torque. The stall torque is about 50 *mNm* which agrees well with the value in the table. Figures 4.4 and 4.5 show the torque-speed plot and the armature current. All values are close to the actual values in table 4.1.

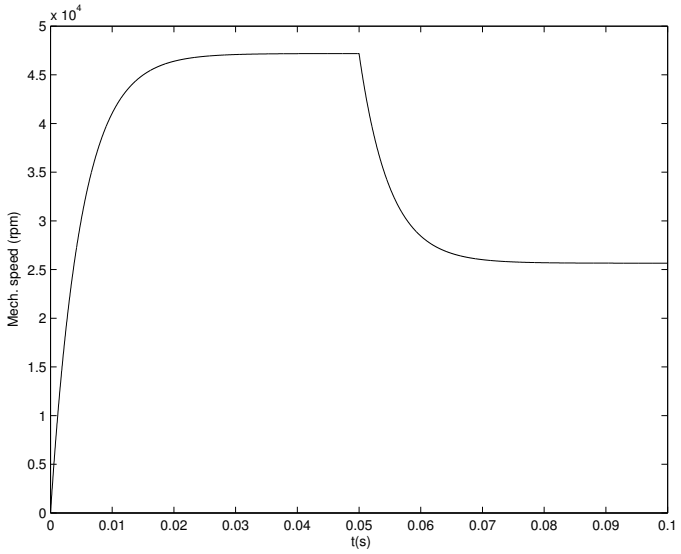

Figure 4.2: DC motor speed

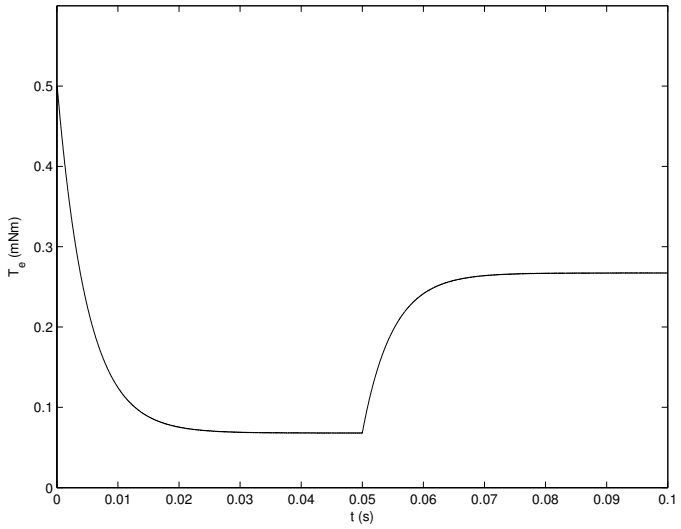

Figure 4.3: Electrical torque of the dc motor

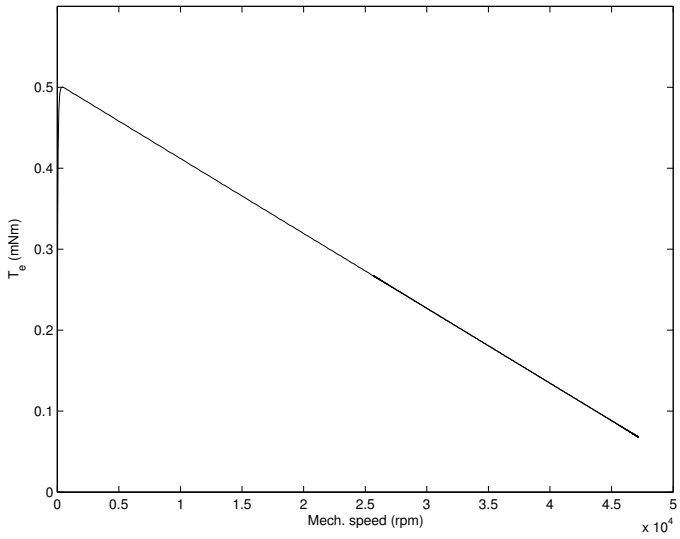

Figure 4.4: Torque-speed plot of the dc motor

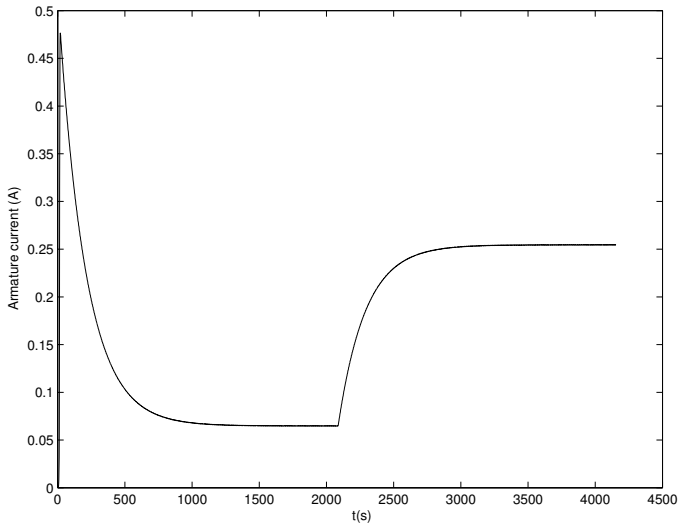

Figure 4.5: DC-link current

4.2 The BLDC motor

4.2.1 The motor

Figure 4.6 shows the complete bldc drive Simulink® model. The core of the bldc motor block is a state-space block that implements the state-space matrix equation 3.12.

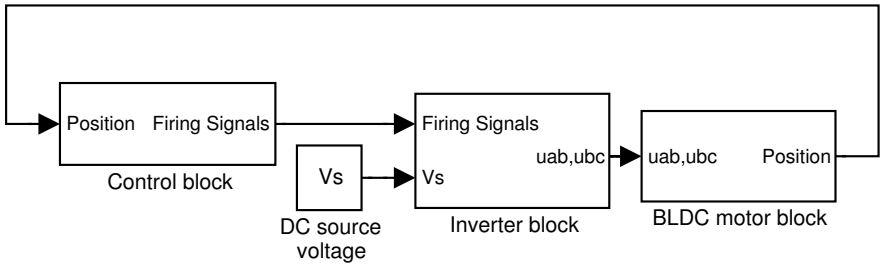

Figure 4.6: The bldc drive model

Figure 4.7 shows the contents of the bldc motor block. The state-space block takes in the difference between the electrical torque and the mechanical torque and two voltage signals from the inverter. The inverter voltages are explained in detail in section 4.2.2. The trapezoidal functions and the position signals are stored in lookup tables that change their output according to the value of the electrical angle as shown in figure 4.8. The electrical torque is calculated as shown in figure 4.9. The electrical position, represented as integer numbers 0-5, is fed to the control block which gives out the firing signals to the inverter. As figure 4.7 shows, the back-emf's and a signal indicating if the phase currents are zero or non-zero, are sent from the motor to the inverter through two Goto blocks. The reason why the inverter needs these signals is explained in section 4.2.2.

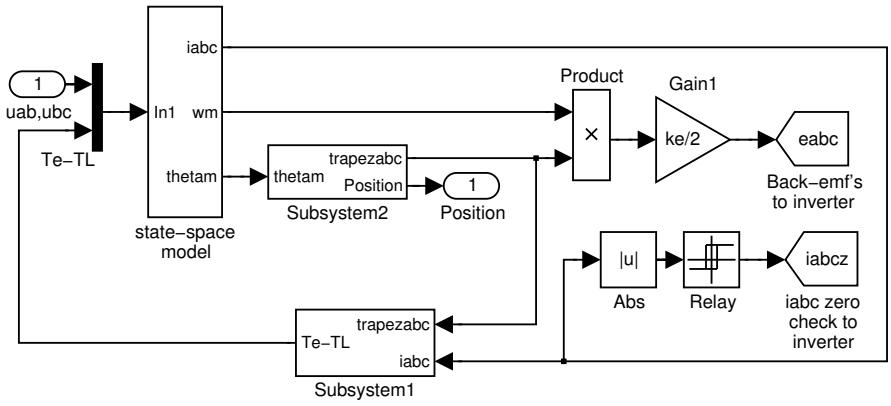

Figure 4.7: Contents of the bldc motor block

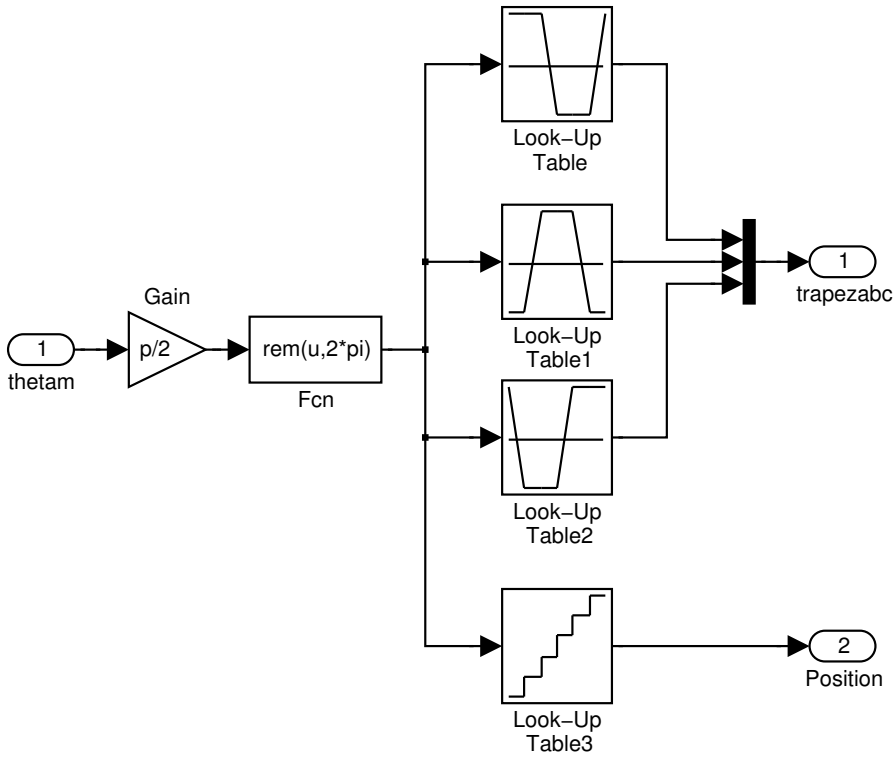

Figure 4.8: Calculation of trapezoidal waveforms and position signals in Subsystem2

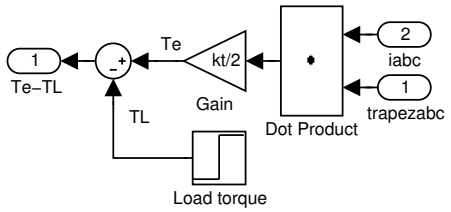

Figure 4.9: Torque calculation in Subsystem1

4.2.2 The Inverter

Output Voltages without a Chopping Signal

The inverter is implemented as an s-function that takes in the value of the dc-source voltage and the firing signals from the control block. The firing signals include a chopping option, i.e. the current in the two energized phases can be turned on and off anytime during the 60° interval. This feature will be used for hysteresis- and pwm control. It will be shown below that the output voltages of the inverter not only depend on the dc-source voltage and the rotor position, but also on the value of the back emf's and whether the phase currents are zero or nonzero.

Figure 4.10 shows how the circuit in figure 3.4 looks like in each 60° interval when the switches are fired according to the sequence in table 3.1. The switches and the diodes are assumed to be ideal devices.

A phase current that is being turned off will flow through a freewheeling diode while the current in the phase that is being turned on is rising from zero. Which phase current is decaying and which one is rising depends on the rotor position. The inverter s-function must not only supply one phase-to-phase dc voltage at a time. It must also take care of the freewheeling diode current and make sure that it can only flow in one direction. By looking at the $0 - 60°$ interval in figure 4.10 it is clear that when the diode current is nonzero, the phase-to-phase voltages are $v_{ab} = v_s$, $v_{bc} = 0$ and $v_{ca} = -V_s$. When the diode current has reached zero, the voltages v_{bc} and v_{ca} will have a different value which depends on the back emf's. In practice these two voltages are not important but since the motor state-space model requires two voltages (v_{ab} and v_{bc}), these two voltages must be known at all times.

The two circuit topologies in figure 4.10 have been redrawn in figure 4.11 where the phases are numbered 1,2 and 3. The back emf's are shown here as voltage sources e_1, e_2 and e_3, and the voltage source v_{d3} acts as a diode.

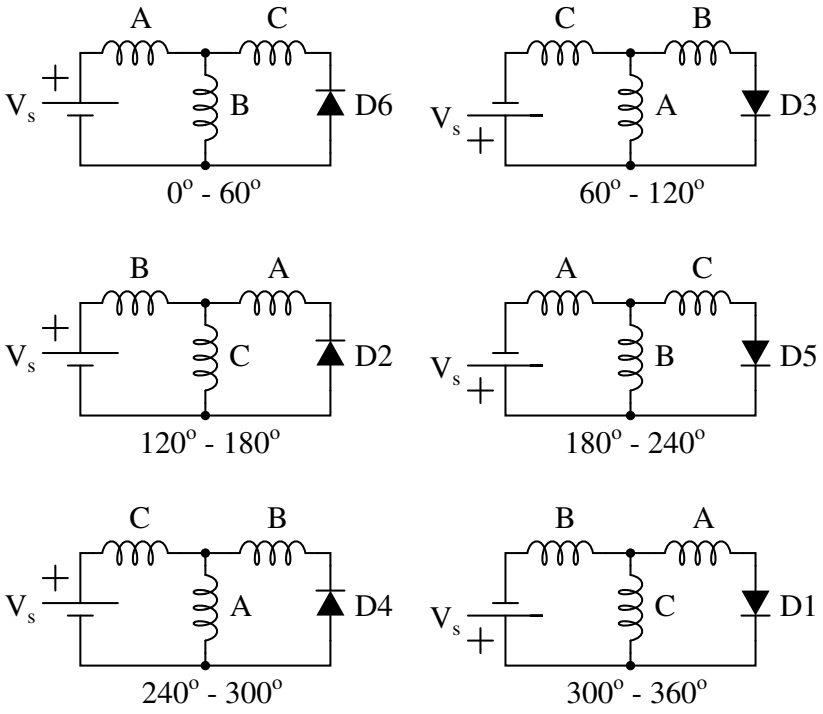

Figure 4.10: Circuit configuration in each 60° interval

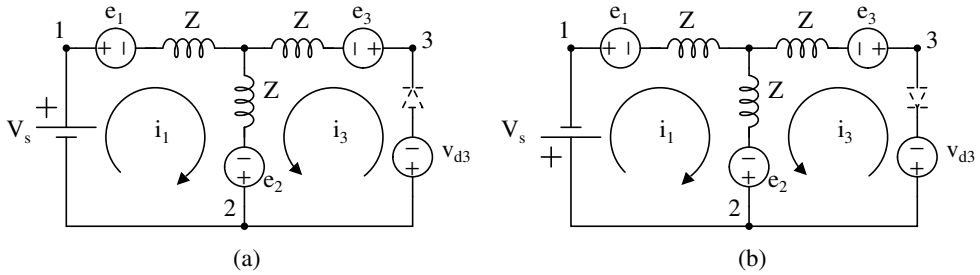

Figure 4.11: The two circuit topologies from figure 4.10

When the diode current is nonzero, the value of v_{d3} is zero but when the diode current has reached zero, v_{d3} must generate a voltage that forces the current to remain at zero until the next interval starts. This value of v_{d3} can be found by inspection or by calculating i_3 as a function of the voltage sources, setting it equal to zero and solving for v_{d3}. For the circuit in figure 4.11(a) the phase-to-phase voltages become

$$i_3 \neq 0 \Rightarrow \begin{cases} v_{12} &= V_s \\ v_{23} &= 0 \\ v_{31} &= -V_s \end{cases}$$

$$i_3 = 0 \Rightarrow \begin{cases} v_{12} &= V_s \\ v_{23} &= \frac{1}{2}(-V_s + e_1 + e_2 - 2e_3) \\ v_{31} &= \frac{1}{2}(-V_s - e_1 - e_2 + 2e_3) \end{cases}$$

and in figure 4.11(b) they are

$$i_3 \neq 0 \Rightarrow \begin{cases} v_{12} &= -V_s \\ v_{23} &= 0 \\ v_{31} &= V_s \end{cases}$$

$$i_3 = 0 \Rightarrow \begin{cases} v_{12} &= -V_s \\ v_{23} &= \frac{1}{2}(V_s + e_1 + e_2 - 2e_3) \\ v_{31} &= \frac{1}{2}(V_s - e_1 - e_2 + 2e_3) \end{cases}$$

Note that the sum of the voltages is always zero and that the only difference between the voltages of circuits (a) and (b) is the sign of V_s.

If the phase-to-phase voltages are to be supplied entirely by the inverter, the inverter s-function must not only know when a diode current reaches zero, it must also know the value of all three back-emf's. As described in section 3.3 the two input voltages of the motor state-space model are the difference between the phase-to-phase voltages and the corresponding phase-to-phase back-emf's. Since the inverter must use the back-emf values to calculate its outputs it is not computationally efficient to add another combination of back-emf's inside the motor block. The inverter is therefore designed to calculate and put out the state-space model input voltages instead of the actual phase-to-phase voltages. The inverter output then becomes

$$i_3 \neq 0 \Rightarrow \begin{cases} u_{12} &= v_{12} - (e_1 - e_2) &= V_s - e_1 + e_2 \\ u_{23} &= v_{23} - (e_2 - e_3) &= -e_2 + e_3 \\ u_{31} &= v_{31} - (e_3 - e_1) &= -V_s - e_3 + e_1 \end{cases}$$

$$i_3 = 0 \Rightarrow \begin{cases} u_{12} &= v_{12} - (e_1 - e_2) &= V_s - e_1 + e_2 \\ u_{23} &= v_{23} - (e_2 - e_3) &= \frac{1}{2}(-V_s + e_1 - e_2) \\ u_{31} &= v_{31} - (e_3 - e_1) &= \frac{1}{2}(-V_s + e_1 - e_2) \end{cases}$$

for the circuit in figure 4.10(a), and

$$i_3 \neq 0 \Rightarrow \begin{cases} u_{12} = v_{12} - (e_1 - e_2) = -V_s - e_1 + e_2 \\ u_{23} = v_{23} - (e_2 - e_3) = -e_2 + e_3 \\ u_{31} = v_{31} - (e_3 - e_1) = V_s - e_3 + e_1 \end{cases}$$

$$i_3 = 0 \Rightarrow \begin{cases} u_{12} = v_{12} - (e_1 - e_2) = -V_s - e_1 + e_2 \\ u_{23} = v_{23} - (e_2 - e_3) = \frac{1}{2}(V_s + e_1 - e_2) \\ u_{31} = v_{31} - (e_3 - e_1) = \frac{1}{2}(V_s + e_1 - e_2) \end{cases}$$

for the circuit in figure 4.10(b). The inverter actually puts out only two voltages but the equations of all three voltages must be known for the derivation of the a,b,c voltages. Now that the voltages u_{12}, u_{23} and u_{31} have been derived, the numbers 1,2,3 are replaced by a,b,c in the appropriate order. The resulting inverter voltages are shown in table 4.2.

Table 4.2: Inverter output voltages

El. Angle	Diode Current	$v_{ab} - e_{ab}$	$v_{bc} - e_{bc}$
$0° - 60°$	$i_c \neq 0$	$V_s - e_a + e_b$	$-e_b + e_c$
	$i_c = 0$	$V_s - e_a + e_b$	$\frac{1}{2}(-V_s + e_a - e_b)$
$60° - 120°$	$i_b \neq 0$	$-e_a + e_b$	$V_s - e_b + e_c$
	$i_b = 0$	$\frac{1}{2}(V_s - e_a + e_c)$	$\frac{1}{2}(V_s - e_a + e_c)$
$120° - 180°$	$i_a \neq 0$	$-V_s - e_a + e_b$	$V_s - e_b + e_c$
	$i_a = 0$	$\frac{1}{2}(-V_s + e_b - e_c)$	$V_s - e_b + e_c$
$180° - 240°$	$i_c \neq 0$	$-V_s - e_a + e_b$	$-e_b + e_c$
	$i_c = 0$	$-V_s - e_a + e_b$	$\frac{1}{2}(V_s + e_a - e_b)$
$240° - 300°$	$i_b \neq 0$	$-e_a + e_b$	$-V_s - e_b + e_c$
	$i_b = 0$	$\frac{1}{2}(-V_s - e_a + e_c)$	$\frac{1}{2}(-V_s - e_a + e_c)$
$300° - 360°$	$i_a \neq 0$	$V_s - e_a + e_b$	$-V_s - e_b + e_c$
	$i_a = 0$	$\frac{1}{2}(V_s + e_b - e_c)$	$-V_s - e_b + e_c$

Inverter Voltages with a Hard Chopping Signal

In hysteresis- and pwm control the current in the energized phases is turned on and off, usually at a high rate. This is called chopping. Hard chopping means that the upper and lower switch are driven by the same chopping signal. Another way of chopping is soft chopping. In soft chopping, only the upper switch is driven by the chopping signal and the lower switch is left on

during the whole interval. The advantage of soft chopping is that it creates less current ripple than the hard chopping technique and switching losses are also lower. The disadvantage is that soft chopping requires more expensive hardware [7].

Figure 4.12 shows the circuit configuration in each interval during hard chopping. Now there are up to three diodes conducting at the same time. Figure 4.13 shows the two circuit topologies that are used to calculate the inverter voltages. The voltage sources v_{d1} and v_{d3} act as diodes and the inverter voltages are calculated as before, i.e. either by inspection or by deriving equations for the two currents i_1 and i_3, setting one of them or both equal to zero and solving for the diode voltage sources. The resulting voltages are shown in table 4.3.

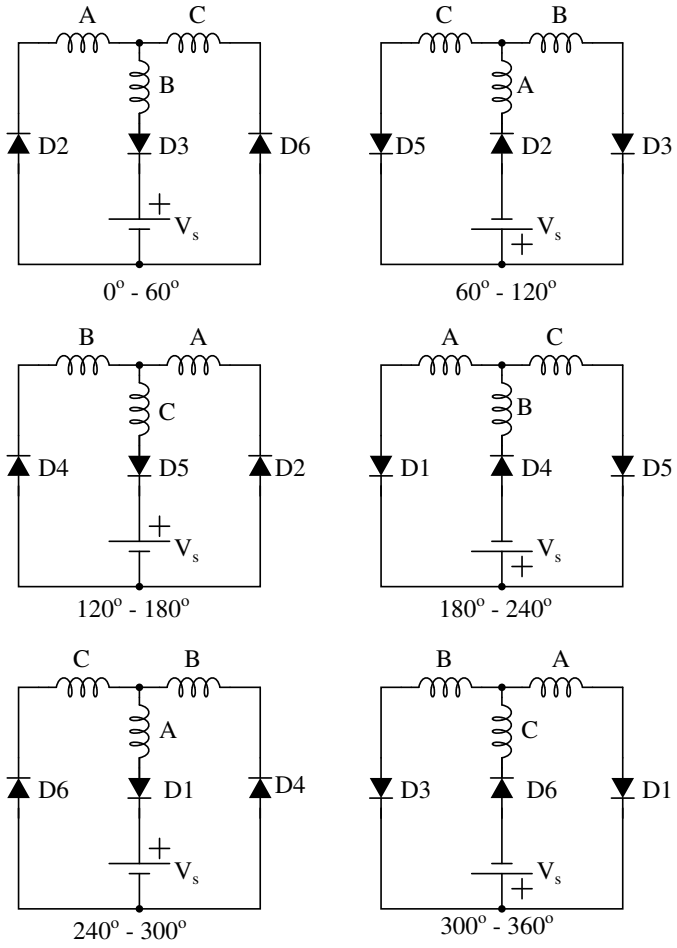

Figure 4.12: Circuit configuration during hard chopping

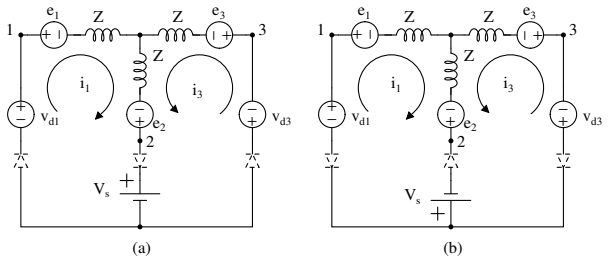

Figure 4.13: The two circuit topologies from figure 4.12

Table 4.3: BLDC motor input voltages during hard chopping

El. Angle	Diode Current	$v_{ab} - e_{ab}$	$v_{bc} - e_{bc}$
$0° - 60°$	$i_a \neq 0, i_c \neq 0$	$-V_s - e_a + e_b$	$V_s - e_b + e_c$
	$i_a \neq 0, i_c = 0$	$-V_s - e_a + e_b$	$\frac{1}{2}(V_s + e_a - e_b)$
	$i_a = 0, i_c \neq 0$	$\frac{1}{2}(-V_s + e_b - e_c)$	$V_s - e_b + e_c$
	$i_a = 0, i_c = 0$	0	0
$60° - 120°$	$i_c \neq 0, i_b \neq 0$	$-V_s - e_a + e_b$	$-e_b + e_c$
	$i_c \neq 0, i_b = 0$	$\frac{1}{2}(-V_s - e_a + e_c)$	$\frac{1}{2}(-V_s - e_a + e_c)$
	$i_c = 0, i_b \neq 0$	$-V_s - e_a + e_b$	$\frac{1}{2}(V_s + e_a - e_b)$
	$i_c = 0, i_b = 0$	0	0
$120° - 180°$	$i_b \neq 0, i_a \neq 0$	$-e_a + e_b$	$-V_s - e_b + e_c$
	$i_b \neq 0, i_a = 0$	$\frac{1}{2}(V_s + e_b - e_c)$	$-V_s - e_b + e_c$
	$i_b = 0, i_a \neq 0$	$\frac{1}{2}(-V_s - e_a + e_c)$	$\frac{1}{2}(-V_s - e_a + e_c)$
	$i_b = 0, i_a = 0$	0	0
$180° - 240°$	$i_a \neq 0, i_c \neq 0$	$V_s - e_a + e_b$	$-V_s - e_b + e_c$
	$i_a \neq 0, i_c = 0$	$V_s - e_a + e_b$	$\frac{1}{2}(-V_s + e_a - e_b)$
	$i_a = 0, i_c \neq 0$	$\frac{1}{2}(V_s - e_b + e_c)$	$-V_s - e_b + e_c$
	$i_a = 0, i_c = 0$	0	0
$240° - 300°$	$i_c \neq 0, i_b \neq 0$	$V_s - e_a + e_b$	$-e_b + e_c$
	$i_c \neq 0, i_b = 0$	$\frac{1}{2}(V_s - e_a + e_c)$	$\frac{1}{2}(V_s - e_a + e_c)$
	$i_c = 0, i_b \neq 0$	$V_s - e_a + e_b$	$\frac{1}{2}(-V_s + e_a - e_b)$
	$i_c = 0, i_b = 0$	0	0
$300° - 360°$	$i_b \neq 0, i_a \neq 0$	$-e_a + e_b$	$V_s - e_b + e_c$
	$i_b \neq 0, i_a = 0$	$\frac{1}{2}(-V_s + e_b - e_c)$	$V_s - e_b + e_c$
	$i_b = 0, i_a \neq 0$	$\frac{1}{2}(V_s - e_a + e_c)$	$\frac{1}{2}(V_s - e_a + e_c)$
	$i_b = 0, i_a = 0$	0	0

Inverter Voltages with a Soft Chopping Signal

When soft chopping is applied, the circuit looks as shown in figure 4.14. The inverter voltages are calculated as before, now using the two circuits in figure 4.15. The resulting voltages are shown in table 4.4.

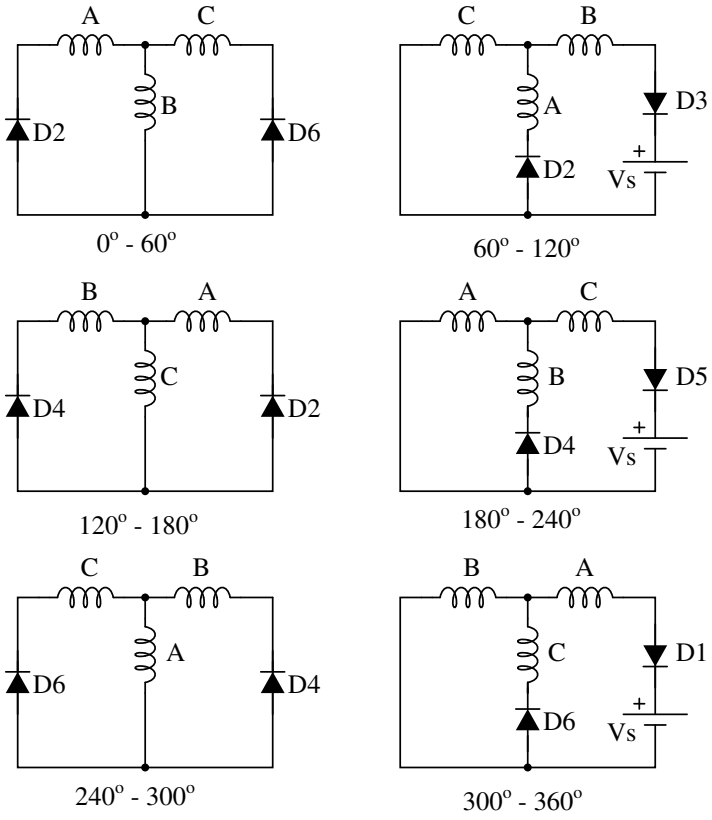

Figure 4.14: Circuit configuration during soft chopping

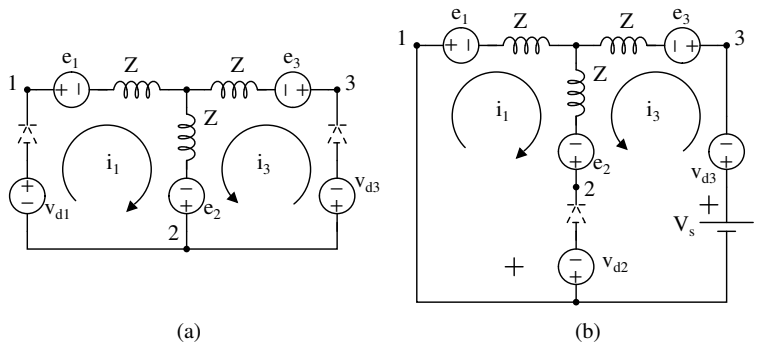

Figure 4.15: The two circuit topologies from figure 4.14

Table 4.4: BLDC motor input voltages during soft chopping

El. Angle	Diode Current	$v_{ab} - e_{ab}$	$v_{bc} - e_{bc}$
$0° - 60°$	$i_a \neq 0, i_c \neq 0$	$-e_a + e_b$	$-e_b + e_c$
	$i_a \neq 0, i_c = 0$	$-e_a + e_b$	$\frac{1}{2}(e_a - e_b)$
	$i_a = 0, i_c \neq 0$	$\frac{1}{2}(e_b - e_c)$	$-e_b + e_c$
	$i_a = 0, i_c = 0$	0	0
$60° - 120°$	$i_a \neq 0, i_b \neq 0$	$-V_s - e_a + e_b$	$V_s - e_b + e_c$
	$i_a \neq 0, i_b = 0$	$\frac{1}{2}(-e_a + e_c)$	$\frac{1}{2}(-e_a + e_c)$
	$i_a = 0, i_b \neq 0$	$\frac{1}{2}(-V_s + e_b - e_c)$	$V_s - e_b + e_c$
	$i_a = 0, i_b = 0$	0	0
$120° - 180°$	$i_b \neq 0, i_a \neq 0$	$-e_a + e_b$	$-e_b + e_c$
	$i_b \neq 0, i_a = 0$	$\frac{1}{2}(e_b - e_c)$	$-e_b + e_c$
	$i_b = 0, i_a \neq 0$	$\frac{1}{2}(-e_a + e_c)$	$\frac{1}{2}(-e_a + e_c)$
	$i_b = 0, i_a = 0$	0	0
$180° - 240°$	$i_b \neq 0, i_c \neq 0$	$-e_a + e_b$	$-V_s - e_b + e_c$
	$i_b \neq 0, i_c = 0$	$-e_a + e_b$	$\frac{1}{2}(e_a - e_b)$
	$i_b = 0, i_c \neq 0$	$\frac{1}{2}(-V_s - e_a + e_c)$	$\frac{1}{2}(-V_s - e_a + e_c)$
	$i_b = 0, i_c = 0$	0	0
$240° - 300°$	$i_c \neq 0, i_b \neq 0$	$-e_a + e_b$	$-e_b + e_c$
	$i_c \neq 0, i_b = 0$	$\frac{1}{2}(-e_a + e_c)$	$\frac{1}{2}(-e_a + e_c)$
	$i_c = 0, i_b \neq 0$	$-e_a + e_b$	$\frac{1}{2}(e_a - e_b)$
	$i_c = 0, i_b = 0$	0	0
$300° - 360°$	$i_c \neq 0, i_a \neq 0$	$V_s - e_a + e_b$	$-e_b + e_c$
	$i_c \neq 0, i_a = 0$	$\frac{1}{2}(e_b - e_c)$	$-e_b + e_c$
	$i_c = 0, i_a \neq 0$	$V_s - e_a + e_b$	$\frac{1}{2}(-V_s + e_a - e_b)$
	$i_c = 0, i_a = 0$	0	0

4.2.3 Simulation

The parameters of the bldc motor model are the same as used in the dc motor model (see table 4.1 page 15). The simulation time and the load torque time and magnitude are also the same. The rotor speed is shown in figure 4.16. The speed curve is identical to the dc motor speed curve. The electrical torque is shown in figure 4.17. As the zoomed view displayed in figure 4.18 shows, the torque has deep but narrow notches.

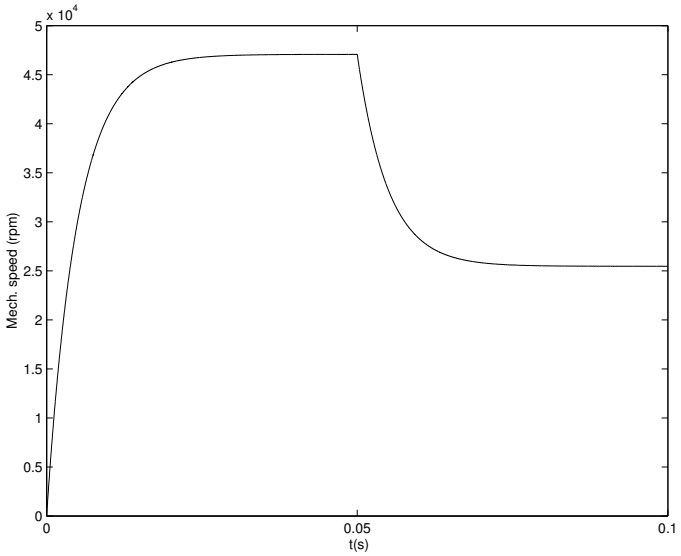

Figure 4.16: Rotor speed

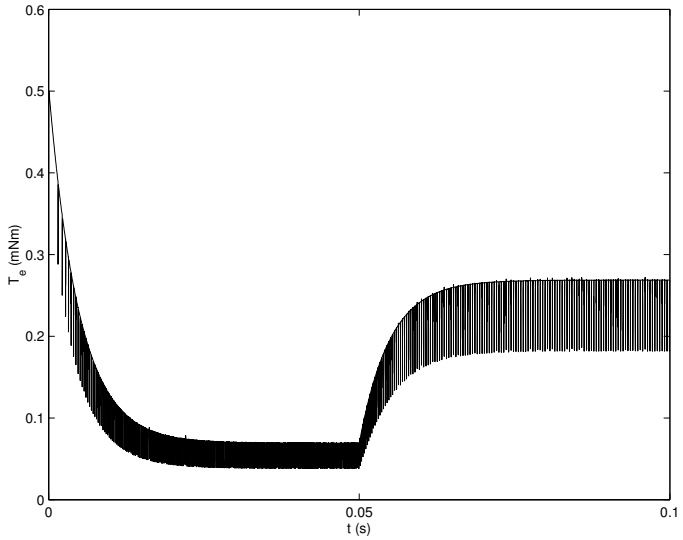

Figure 4.17: Electrical torque

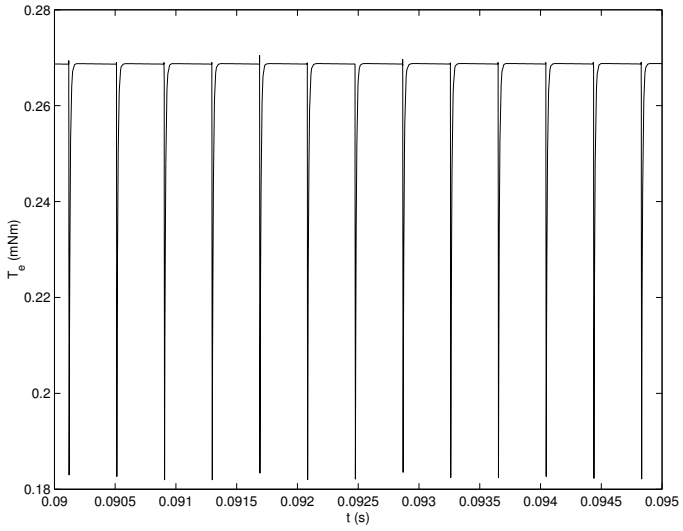

Figure 4.18: Zoomed view of the electrical torque

A plot of torque vs. speed is shown in figure 4.19. The torque-speed characteristics follow a straight line identical of the one of the dc motor with the exception of the points where notches occur in the torque. The stall torque is 0.50 mNm which is in accordance with the motor data.

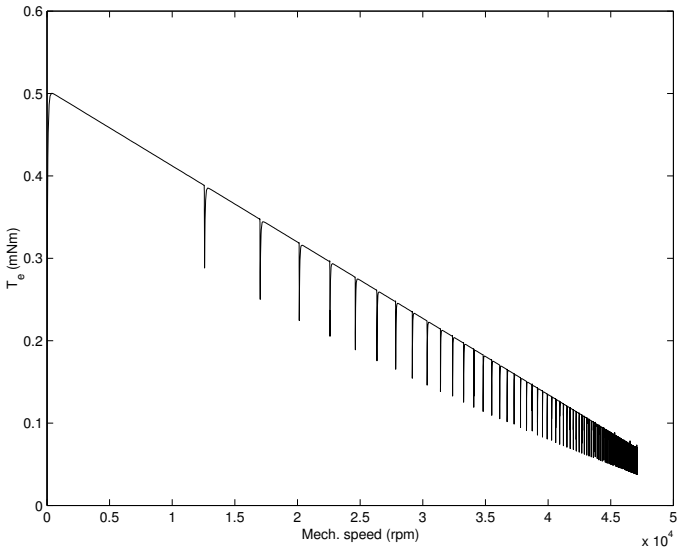

Figure 4.19: Torque-speed plot

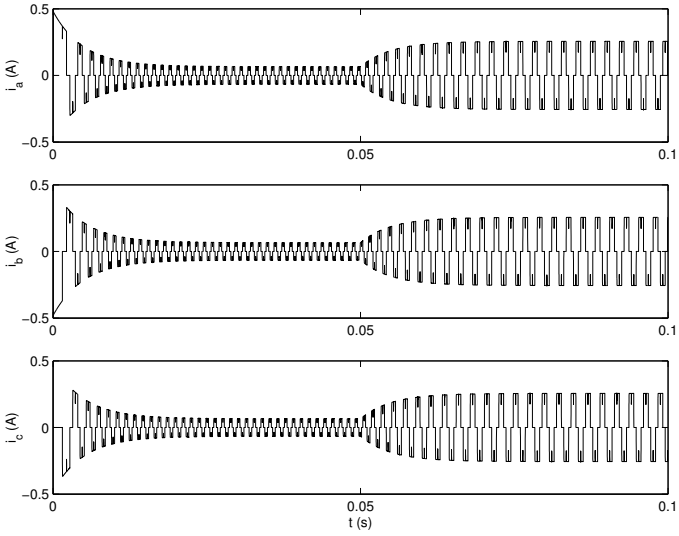

Figure 4.20: Phase currents

Figure 4.20 shows the phase currents. The current starts with a high value and decays as the motor speeds up until it reaches the no-load current which is about 60 mA which agrees with the value in table 4.1. The current rises again when the load torque is applied and reaches a steady state value of 250 mA. Figure 4.21 shows a zoomed view of the phase currents and the back-emf's after the load torque has been applied. The current has a nearly perfect quasi-square wave shape. The only deviation from the quasi-square wave shape occurs at the commutation points. The notches at the commutation points occur because the rise of the current in the phase that is being turned on is slower than the decay of the current in the phase that is being turned off. The notches are the cause of the well known torque ripples of bldc motors.

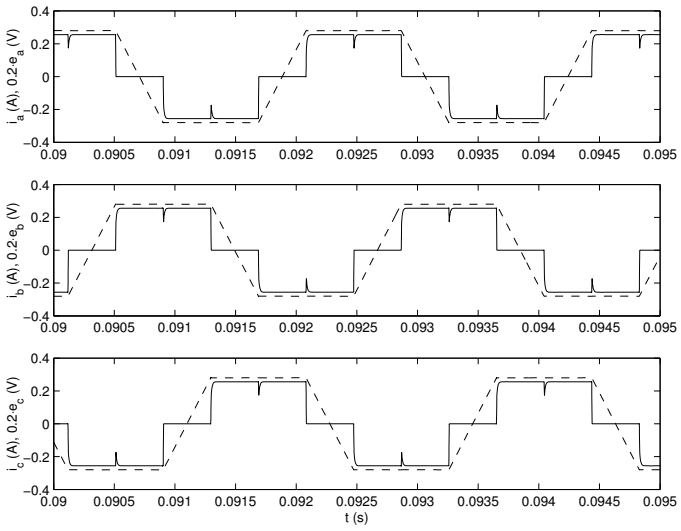

Figure 4.21: Zoomed view of phase currents (solid) and back-emf's (dashed)

The model appears to be correct. The torque-speed relationship is linear and the stall torque, the no-load speed and the no-load current all agree with the values given in the motor's datasheet.

Chapter 5

Control

In this chapter, three different control schemes are tested on the bldc motor. The controlled variables are torque, speed and position. The chapter starts with hysteresis band control followed by pulse width modulation (pwm) control and variable dc-link voltage control. The different methods are tested and the results discussed and compared. The frequency spectrum of the dc-link current is calculated and the effect that the different control techniques have on it is investigated.

5.1 Hysteresis Band Control

Hysteresis band control is one of the simplest closed-loop control schemes. In hysteresis band control, the value of the controlled variable is forced to stay within certain limits (hysteresis band) around a reference value. As an example, to control motor speed, the motor is turned off if the speed reaches a certain level above the reference speed and turned back on when the speed falls below a certain level below the reference speed. The drawback of the hysteresis band control technique are the high and uncontrolled switching frequencies when a narrow hysteresis band is used and large ripples when the hysteresis band is wider [11]. The uncertain switching frequency make filtering of acoustic- and electromagnetic noise difficult [7]. The switching method used here is the soft chopping method, i.e. only the upper switch is turned on and off while the lower switch is left on. This method produces less torque ripple and less switching losses than the hard chopping method. Only torque control and speed control is implemented here. The reason is that if position control were to be implemented in the same way as the torque- and the position control, it would only be possible by constantly reversing the rotor speed so that the rotor angle would stay withing the hysteresis

band. This is not a practical solution and it would put high stress on both mechanical parts and electronic devices.

5.1.1 Torque Control

In this control scheme, as in the ones presented below, only one current controller is used. This strategy, suggested and presented in [3], is simple and avoids difficult sensing of the dc-link current. A signal equivalent to the dc-link current is synthesized from the measurement of two phase currents. A necessary condition for the validity of this method is that the sum of the phase currents is zero. This methods suits the bldc motor used here as it is a three phase star-connected motor with an ungrounded neutral point. A dc-link current reference value is derived from the reference torque using the realationship

$$I_{ref} = \frac{T_{eref}}{k_t}. \tag{5.1}$$

The hysteresis band control is easy to implement with a relay block as shown in figure 5.1. The upper and the lower limits are the reference current plus and minus half of the hysteresis band respectively. When the current reaches the upper limit, the relay block puts out a high signal to the control block which generates chopping signals for the inverter. When the current falls below the lower limit, the output of the relay block is a low signal and the control block stops the chopping operation of the inverter.

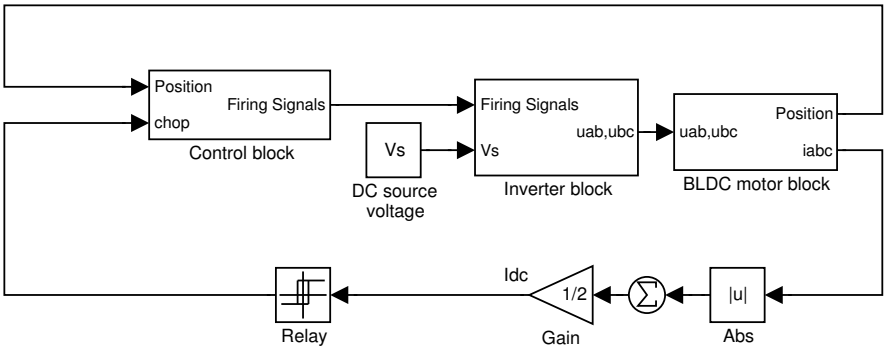

Figure 5.1: Hysteresis torque control system

Figure 5.2 shows the electrical torque when the reference value is 0.2 mNm and load torque equal to the reference value is applied at 0.05 s. Without a torque controller, the electrical torque would reach 0.5 mNm at the start

but it never goes above the upper limit of the hysteresis band. The width of the hysteresis band here is 10% of the reference value. When the load torque is applied, the electrical torque remains the same so the speed falls down to zero as shown in figure 5.3. In this case the commutation ripples are no longer a problem. The ripples produced by this control strategy have a much larger impact, especially when the hysteresis band is wide. Figure 5.4 shows the phase currents.

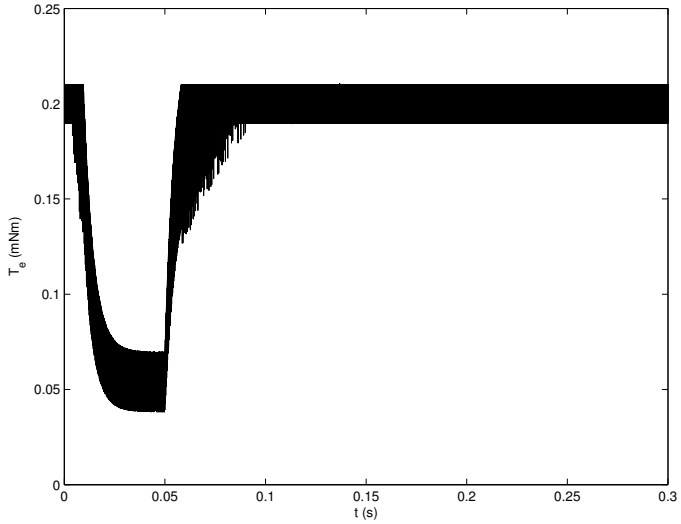

Figure 5.2: Electrical torque in hysteresis torque control exposed to a load-step

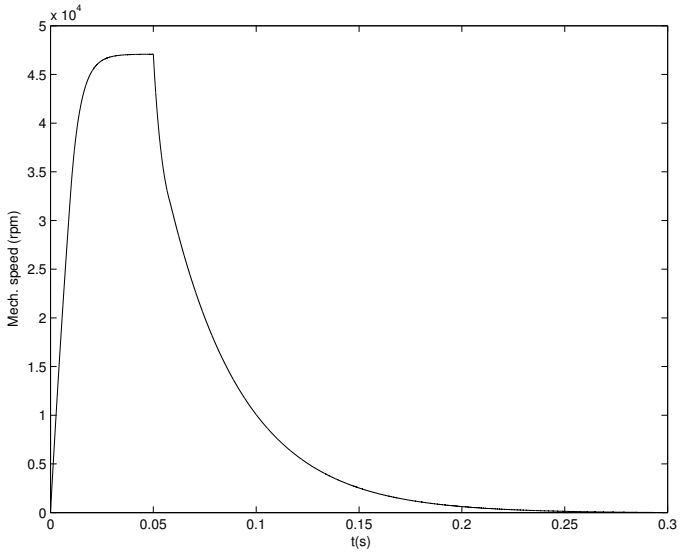

Figure 5.3: Rotor speed in hysteresis torque control exposed to a loadstep

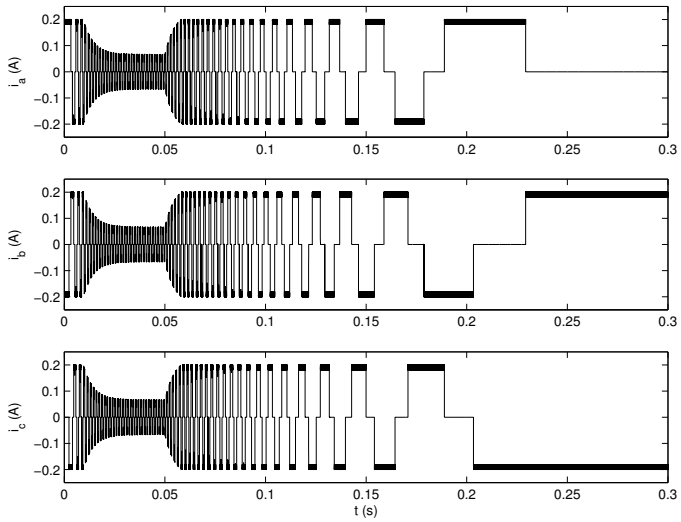

Figure 5.4: Phase currents in hysteresis torque control exposed to a loadstep

5.1.2 Speed Control

Figure 5.5 shows the bldc motor with a hysteresis speed controller. The principle is similar to the one in the torque control scheme described in the previous section. Here the rotor speed is fed to the relay block. The upper and the lower limits of the relay block are in this case the speed reference value plus and minus half of the hysteresis band width respectively. The width of the hysteresis band is now 1% of the reference speed.

The position signal could be used to calculate the rotor speed but the actual rotor speed is used here directly since it is already available from the state-space block. To calculate the position signal from the rotor speed and then calculate the speed from the position signal would be an unnecessary computational burden. I practice, when implementing speed- and position control, high-resolution position sensors are used.

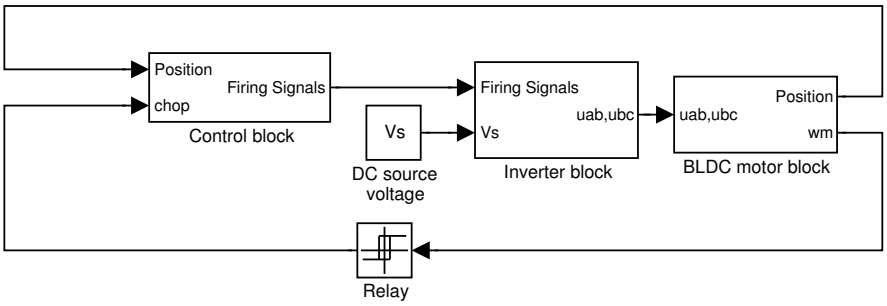

Figure 5.5: Hysteresis speed control system

Figure 5.6 shows the rotor speed when a load torque is appled at 0.01 s. The reference speed is 20,000 rpm and the magnitude of the load is the maximum continuous load allowed (0.23 mNm). As can be seen in the figure, the frequency of the speed ripples increases after the load step. This change of frequency will be investigated in section 5.4. The speed however, stays within the hysteresis band around the reference value.

Figure 5.7 shows the electrical torque. The torque ripples are strong and transiently go all the way down to zero torque. Before the load is applied, the torque is only narrow spikes but when the load is applied, the nonzero time of the period becomes larger than the zero time. The dc-link current is not shown here but it is proportional to the electrical torque and has the same frequency content. Figure 5.8 shows the phase currents.

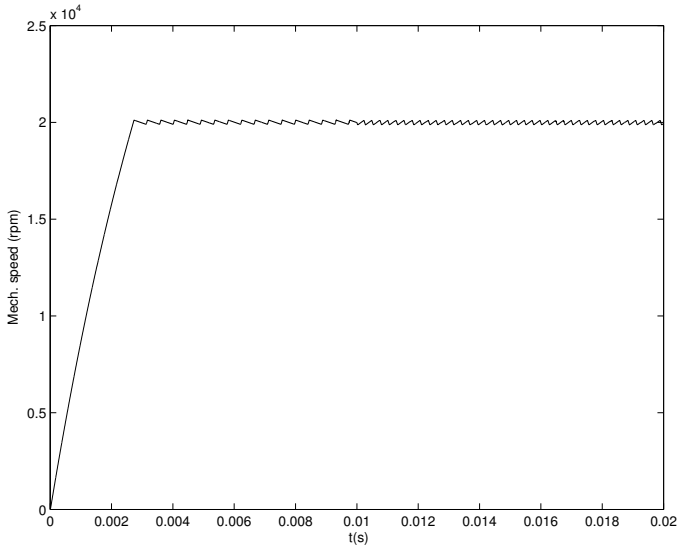

Figure 5.6: Rotor speed in hysteresis speed control exposed to a loadstep

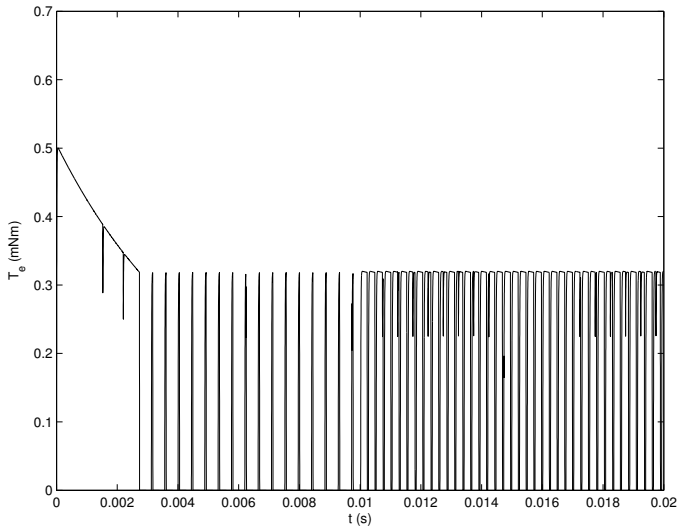

Figure 5.7: Electrial torque in hysteresis speed control exposed to a loadstep

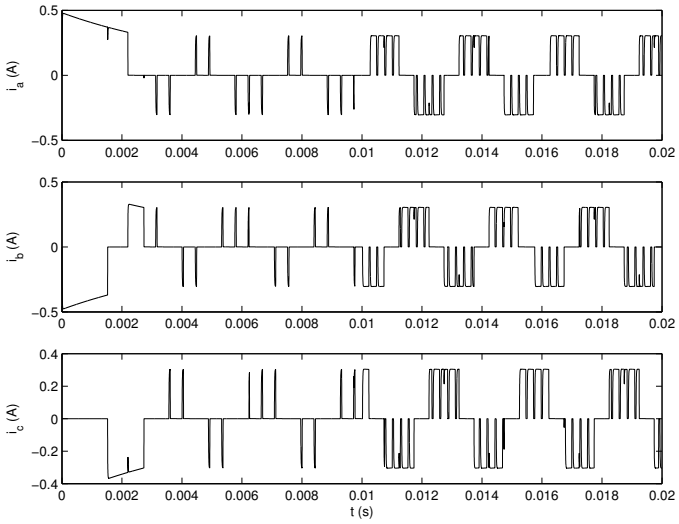

Figure 5.8: Phase currents in hysteresis speed control exposed to a loadstep

5.2 PWM Control

In pwm control the motor is turned on and off at a high rate. The chopping frequency is fixed but the length of the duty cycle depends on the control error. The fact that the frequency is fixed makes filtering of acoustic- and electromagnetic noise easier. The switching frequency is commonly 20-50 kHz and since the motors used here can operate at quite high speed, the frequency is chosen as 50 kHz.

5.2.1 Torque Control

The current control strategy suggested in [3] was briefly described in section 5.1.1. Here the same current sensing method is used so that only one current controller is needed. Figure 5.9 shows the control system. The phase currents are converted to an equivalent dc-link current value. This value is subtracted from a reference value calculated from the torque reference as in section 5.1.1. The current error is fed to a current controller and the output of the controller is compared to a triangular wave. The output of the comparator is a high or low signal which serves as a chopping signal for the inverter.

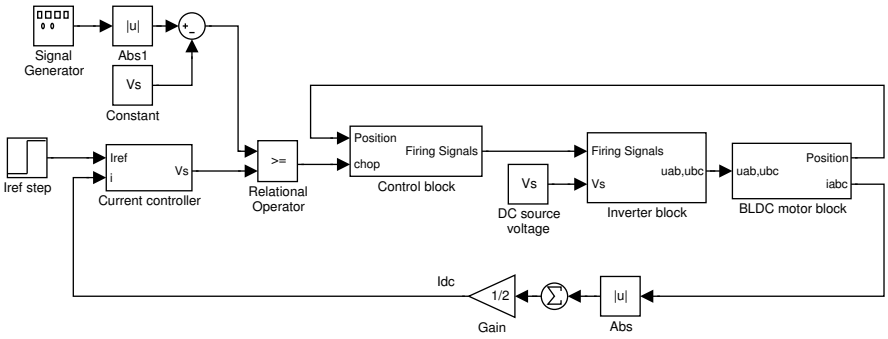

Figure 5.9: PWM torque control system

The current controller is a PI controller and its design is based on a current controller for a dc motor presented in [6]. The design starts by selecting a desired rise time t_{re} for the current. From that, a constant α_e, is determined as

$$\alpha_e = \frac{\ln 9}{t_{re}} \tag{5.2}$$

and the controller parameters follow as

$$k_p = \alpha_e L \tag{5.3}$$

$$k_i = \alpha_e R. \tag{5.4}$$

The selected rise time is 0.1 ms which yields

$$k_p = 2.00 \cdot 10^3$$

$$k_i = 2.75 \cdot 10^5$$

The controller also uses back-calculation to prevent integrator windup (see [6]) and has a voltage saturation block that limits the demanded voltage to ± 6 V so that the comparison with the triangular wave will give correct results. Figure 5.10 shows the electrical torque. The reference torque and the load step is still 0.2 mNm but the torque fluctuation is larger than in the hysteresis control. The reason for this is that the electrical dynamics are very fast compared with the switching frequency.

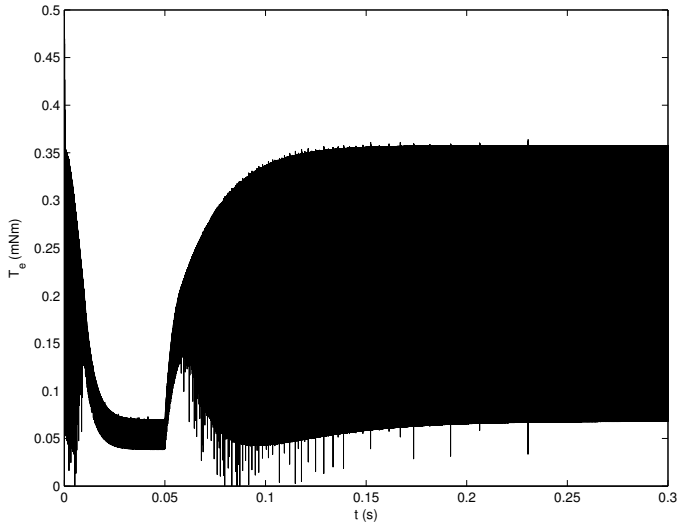

Figure 5.10: Electrical torque in pwm torque control exposed to a loadstep

This can be seen by comparing the phase currents in figures 5.12 and 5.4. The chopping notches go much deeper in the pwm scheme. A higher switching frequency will produce less variation in current and therefore smoother torque. The rotor speed is shown in figure 5.11 and it follows the same curve as the speed in the hysteresis control scheme.

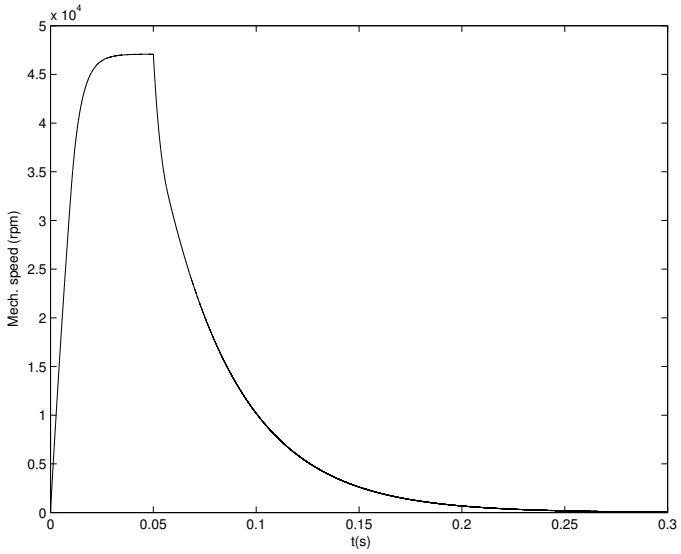

Figure 5.11: Rotor speed in pwm torque control exposed to a loadstep

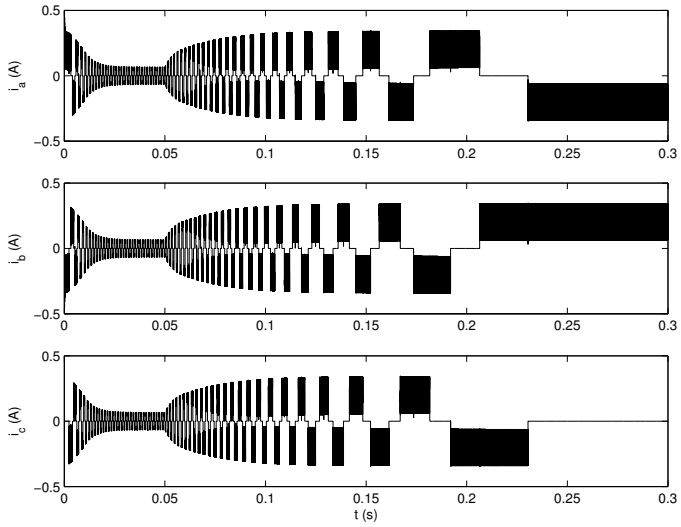

Figure 5.12: Phase currents in pwm torque control exposed to a loadstep

5.2.2 Speed Control

The pwm speed control system is shown in figure 5.13. The current controller is the same as before but a PI speed controller has been added. The speed controller parameters are derived using similar reasoning as for the current controller parameters in [6]. The parameters are calculated as

$$k_p = \alpha_\omega J \tag{5.5}$$

$$k_i = \alpha_\omega k_f \tag{5.6}$$

and α_ω depends on the desired rise time of the speed. Three values of α_ω will be tried here. The first value makes the speed control as fast as the current control, the second makes it hundred times slower and the last values makes it ten times slower.

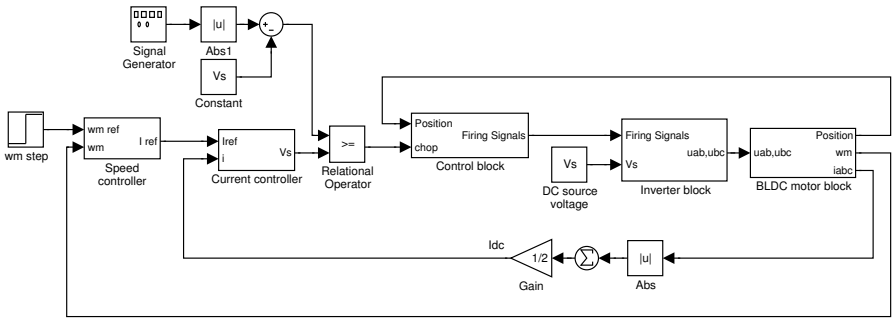

Figure 5.13: PWM speed control system

Setting $\alpha_\omega = \alpha_e$ gives the following parameters:

$$k_p = 1.10 \cdot 10^{-5}$$

$$k_i = 3.03 \cdot 10^{-4}$$

The reference speed is 20,000 rpm as before. Figure 5.14 shows that these control parameters produce a small overshoot in speed and there also appears to be some steady state error. Figures 5.15 and 5.16 show the electrical torque and the phase currents. The pwm duty cycle is 100% until the speed reaches the reference value. The phase currents show that it takes only about one rotor revolution to reach steady state.

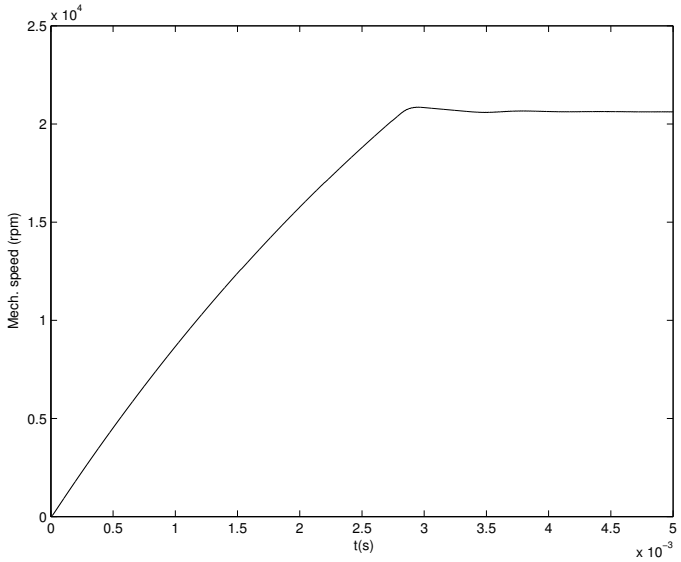

Figure 5.14: Rotor speed in pwm speed control at no load ($\alpha_\omega = \alpha_e$)

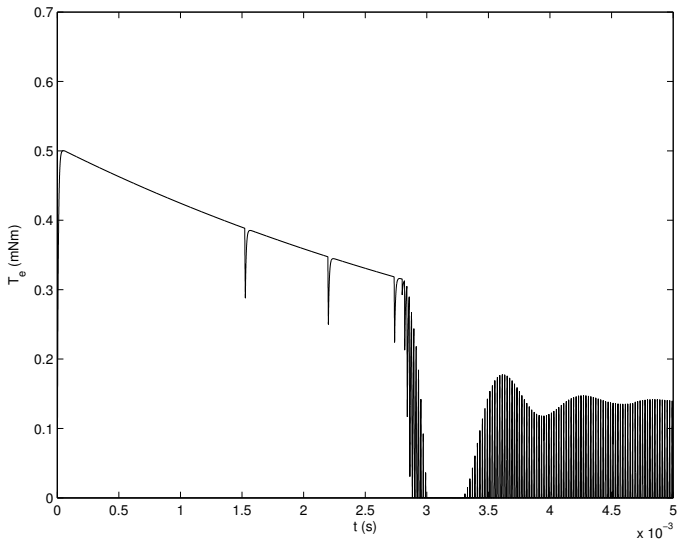

Figure 5.15: Electrical torque in pwm speed control at no load ($\alpha_\omega = \alpha_e$)

Setting $\alpha_\omega = 0.01\alpha_e$ results in a much slower response as shown in figure 5.17. The controller parameters are now

$$k_p = 1.10 \cdot 10^{-7}$$

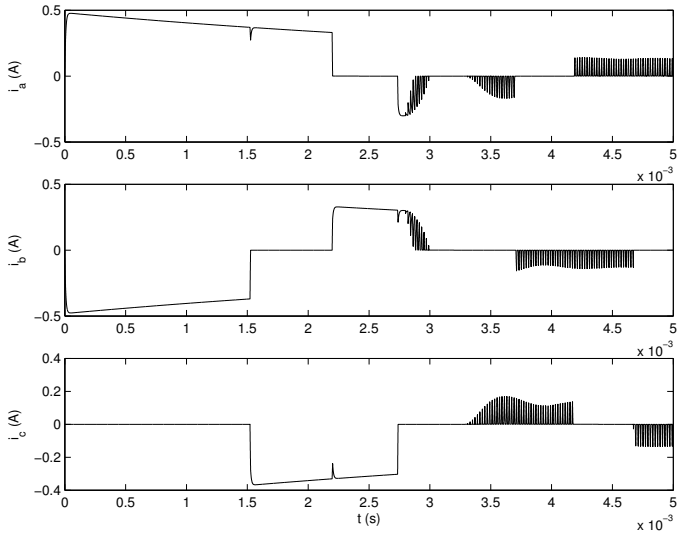

Figure 5.16: Phase currents in pwm speed control at no load ($\alpha_\omega = \alpha_e$)

$$k_i = 3.03 \cdot 10^{-6}$$

There is no overshoot here but the steady state error remains. As figures 5.18 and 5.19 show, the pwm operation begins right at the start in order to slow down the rise of the speed.

Using $\alpha_\omega = \alpha_e$ is too fast and $\alpha_\omega = 0.01\alpha_e$ is slow, so $\alpha_\omega = 0.1\alpha_e$ is used here as a compromise. The resulting control parameters are

$$k_p = 1.10 \cdot 10^{-6}$$

$$k_i = 3.03 \cdot 10^{-5}$$

Figure 5.20 shows that these parameters give better results. There appears to be no overshoot but there is a small steady state error. Using a longer simulation time reveals that there is a small overshoot and the steady state error becomes smaller than the error seen in figure 5.20. Figures 5.21 and 5.22 show the electric torque and the phase currents respectively.

Figure 5.23 shows how the system reacts to a large load step of 0.23 mNm which is the maximum continuous load that can be applied to the motor. The speed drop is considerable.

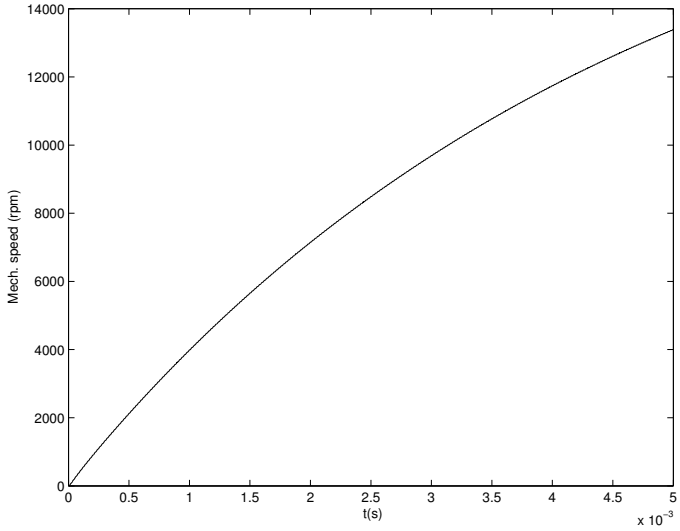

Figure 5.17: Rotor speed in pwm speed control at no load ($\alpha_\omega = 0.01\alpha_e$)

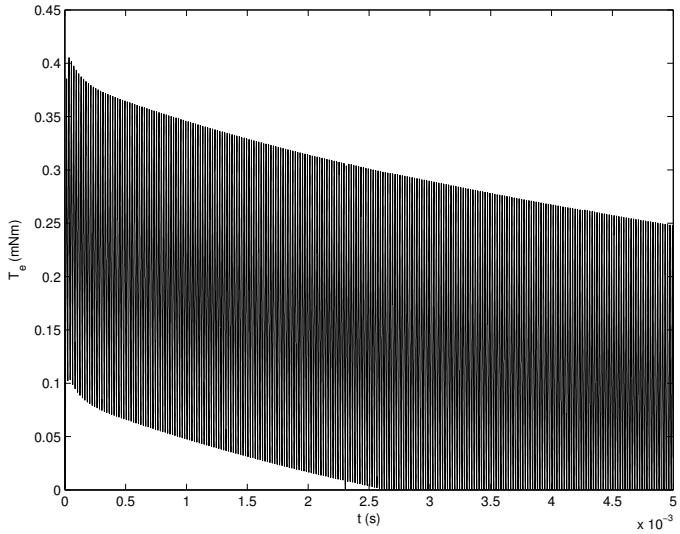

Figure 5.18: Electrial torque in pwm speed control at no load ($\alpha_\omega = 0.01\alpha_e$)

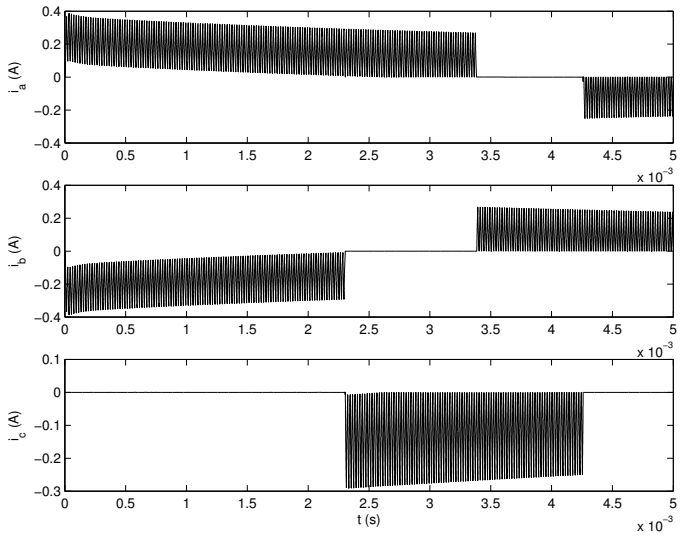

Figure 5.19: Phase currents in pwm speed control at no load ($\alpha_\omega = 0.01\alpha_e$)

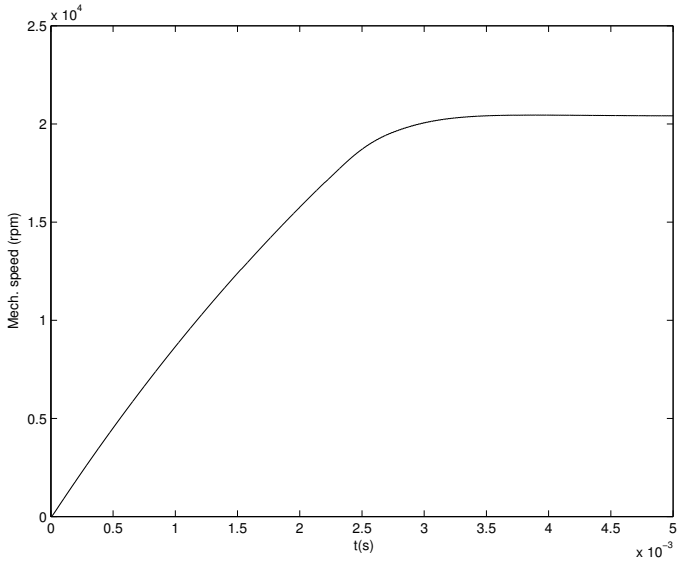

Figure 5.20: Rotor speed in pwm speed control at no load ($\alpha_\omega = 0.1\alpha_e$)

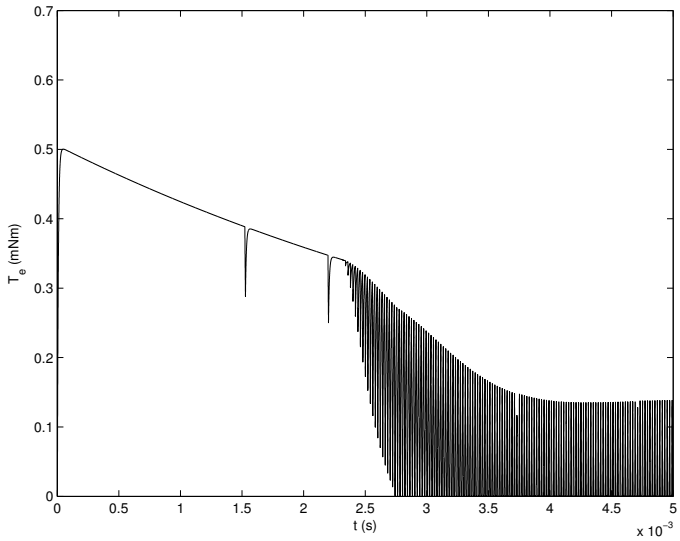

Figure 5.21: Electrical torque in pwm speed control at no load ($\alpha_\omega = 0.1\alpha_e$)

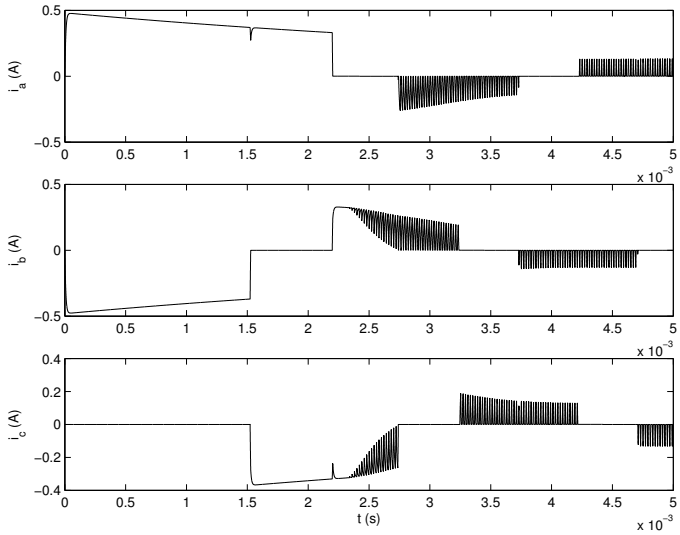

Figure 5.22: Phase currents in pwm speed control at no load ($\alpha_\omega = 0.1\alpha_e$)

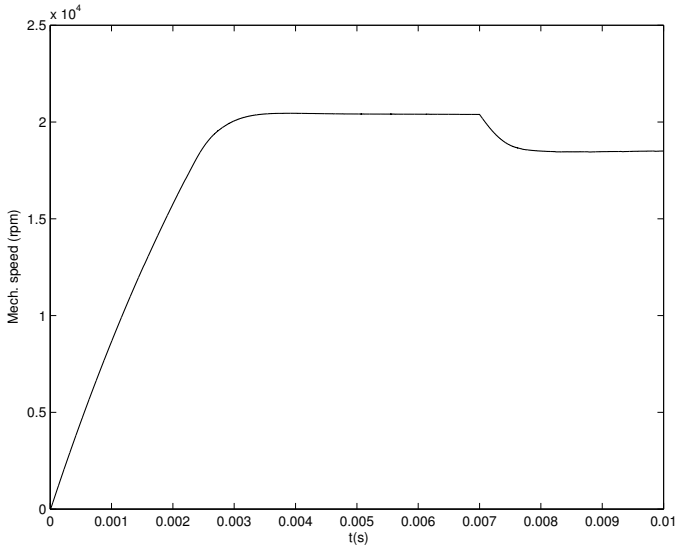

Figure 5.23: Rotor speed in pwm speed control at maximum load step ($\alpha_\omega = 0.1\alpha_e$)

5.2.3 Position Control

The position controller is another PI controller as shown in figure 5.24. The controller can not be very fast because if an overshoot occurs, the only way to go closer down to the reference angle would be to reverse the rotor speed. This bldc motor model does not support speed reversal. The controller is therefore made slow to prevent an overshoot.

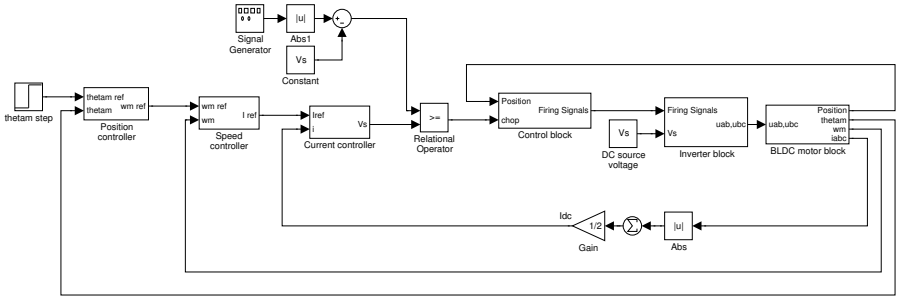

Figure 5.24: PWM position control system

The controller parameters used here are obtained by using the trial and error method. Using

$$k_p = 6.59 \quad \text{and} \quad k_i = 9.10 \cdot 10^{-8}$$

gives the good results. Figure 5.25 shows the rotor angle at no load operation. The reference angle is 3600°. The error is only a fraction of a degree. Figure 5.26 shows the same thing when the maximum continuous load (0.23 mNm) is applied at the start. The results are identical with practically zero error.

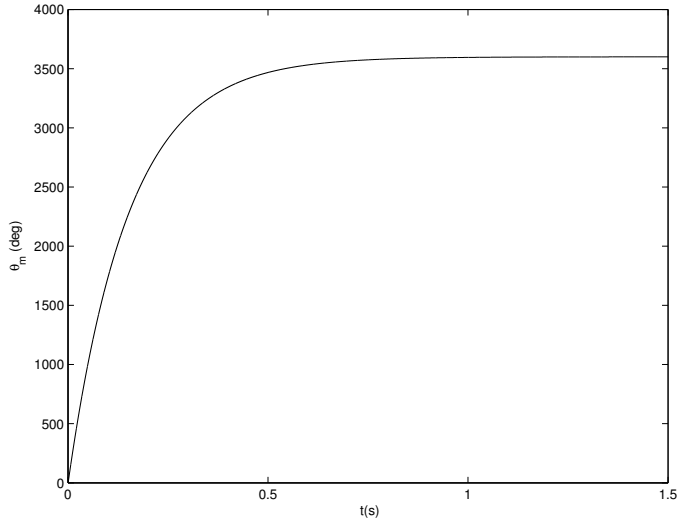

Figure 5.25: Rotor angle in pwm position control at no load

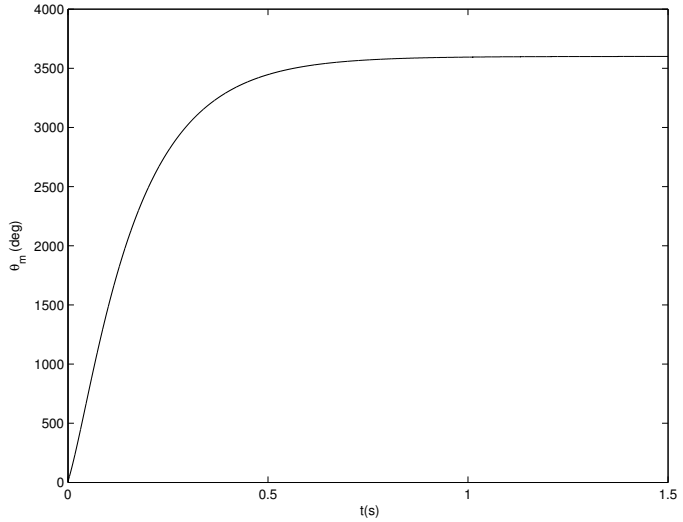

Figure 5.26: Rotor angle in pwm position control at maximum load

5.3 Variable DC-Link Voltage Control

Using a variable dc voltage source to control the applied voltage can have some advantages over the two methods previously discussed. A linear power stage is cheaper than a pulsed power stage (pwm) but the losses can be high at low voltage and high current [12]. However, at high speed, a linear power stage can be the best alternative when switching losses and commutation delay of a pulsed power stage become significant [13].

5.3.1 Torque Control

The torque controller used here is just like the one used for the pwm control except that the output voltage is limited to 0-6 V. The PI constants are the same and the reference torque is the same. Figure 5.27 shows the whole system.

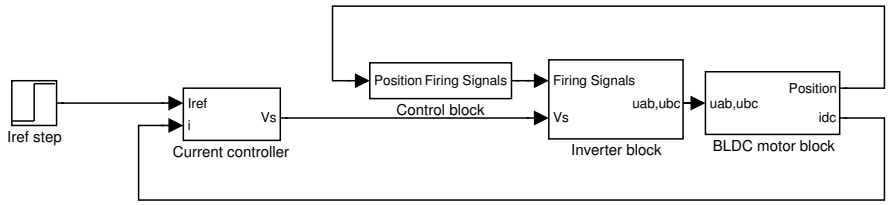

Figure 5.27: Varible dc-link voltage torque control system

Figure 5.28 shows the electrical torque. Now the only irregularites in the torque occur at the commutation instants. The ripples are quite large but very narrow and not as frequent as the ripples in the hysteresis band and pwm control schemes. Figures 5.29 and 5.30 show the rotor speed and the phase currents respectively.

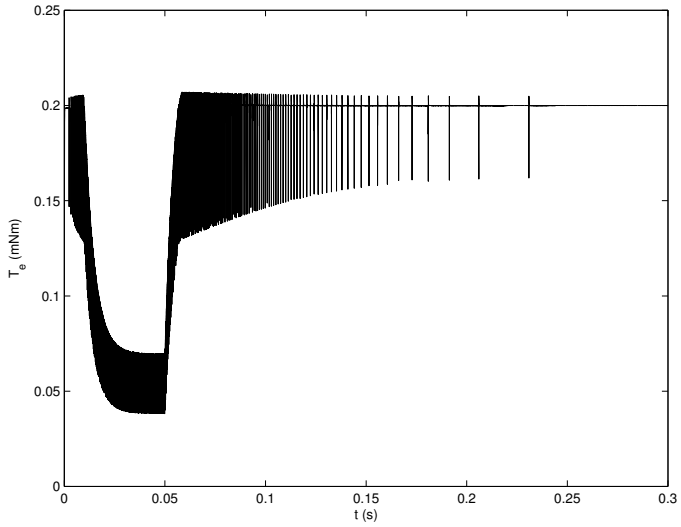

Figure 5.28: Electrical torque in variable dc-link voltage torque control

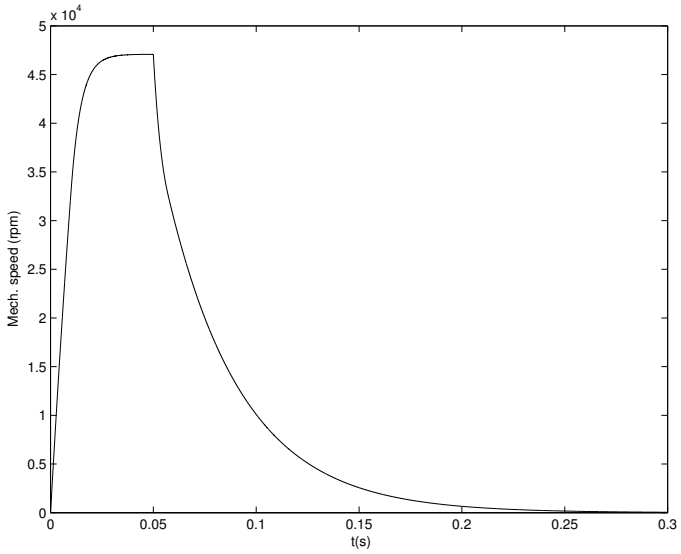

Figure 5.29: Rotor speed in variable dc-link voltage torque control

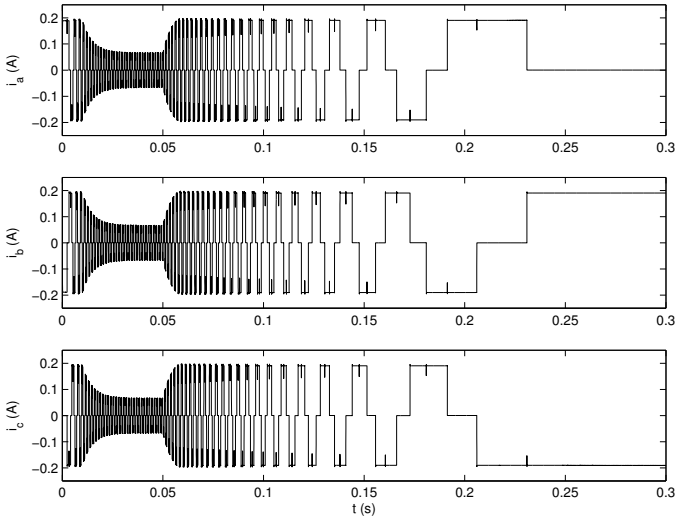

Figure 5.30: Phase currents in variable dc-link voltage torque control

5.3.2 Speed Control

The speed controller used here is the same controller that was used for the pwm speed control. Figure 5.31 shows the whole system. The reference speed is still 20,000 rpm and the same PI constants are used.

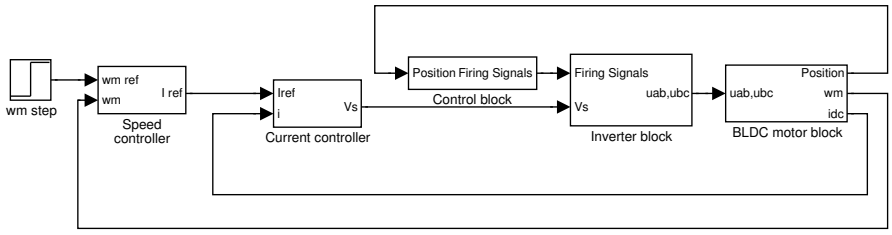

Figure 5.31: Varible dc-link voltage, speed control system

The testing procedure here is the same as in section 5.2.2. The controller is first made very fast which results in a small overshoot as shown in figure 5.32. Figures 5.33 and 5.34 show the electrical torque and the phase currents respectively. It is interesting to note that the electrical torque becomes negative for a short time. This happens when the applied voltage becomes lower than the phase-to-phase back-emf, and current starts to flow to the voltage source through the freewheeling diodes.

Figures 5.35, 5.36 and 5.37 show the same curves when the controller is made very slow ($\alpha_\omega = 0.01\alpha_e$). The results are the same as with the pwm control except that the torque is much smoother.

Figures 5.38, 5.39 and 5.40 show the results when the controller is made faster ($\alpha_\omega = 0.1\alpha_e$). Again the results are similar to results in the pwm control.

Figures 5.41 and 5.42 show how the controller reacts to a large load step (maximum continuous load, 0.23 mNm). The decrease in speed is considerable as with the pwm controller.

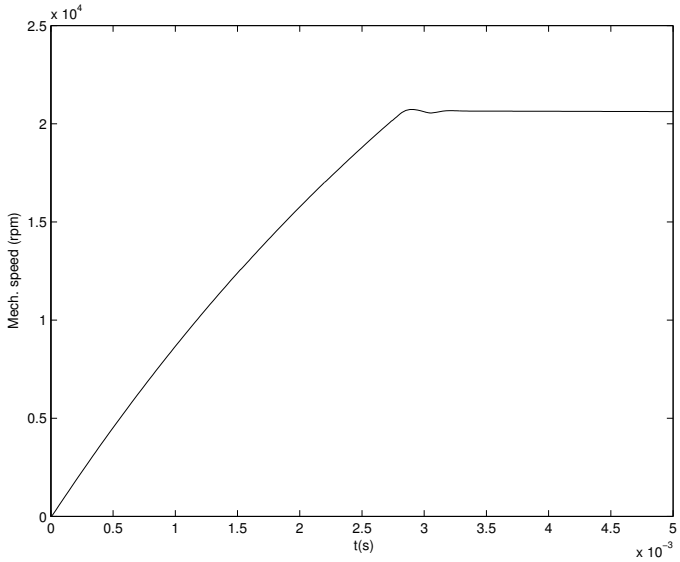

Figure 5.32: Rotor speed in variable dc-link voltage speed control control at no load ($\alpha_\omega = \alpha_e$)

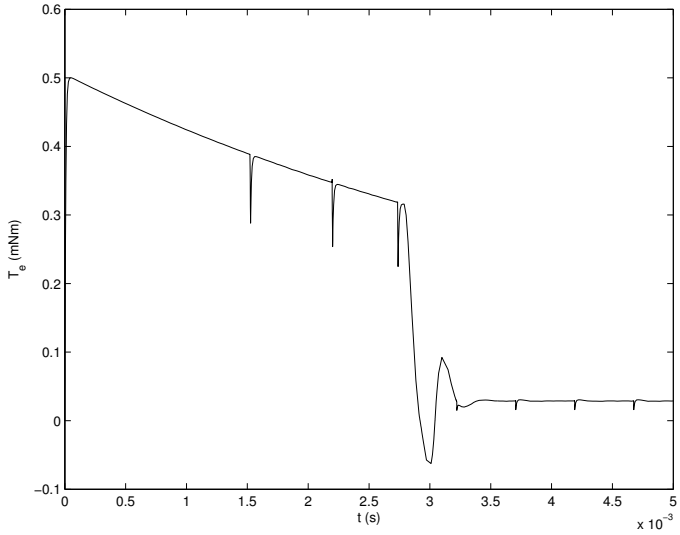

Figure 5.33: Electrical torque in variable dc-link voltage speed control at no load ($\alpha_\omega = \alpha_e$)

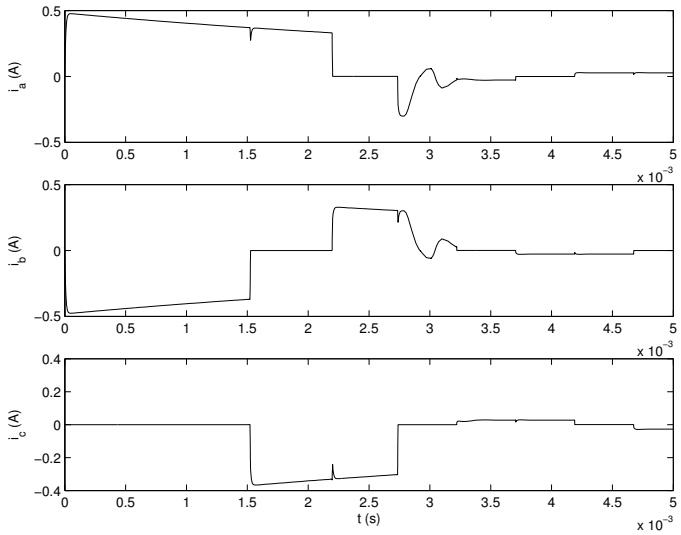

Figure 5.34: Phase currents in variable dc-link voltage speed control at no load ($\alpha_\omega = \alpha_e$)

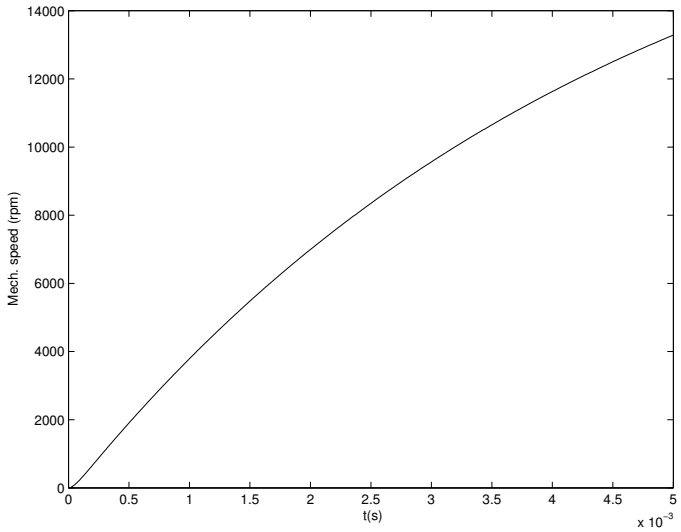

Figure 5.35: Rotor speed in variable dc-link voltage speed control at no load ($\alpha_\omega = 0.01\alpha_e$)

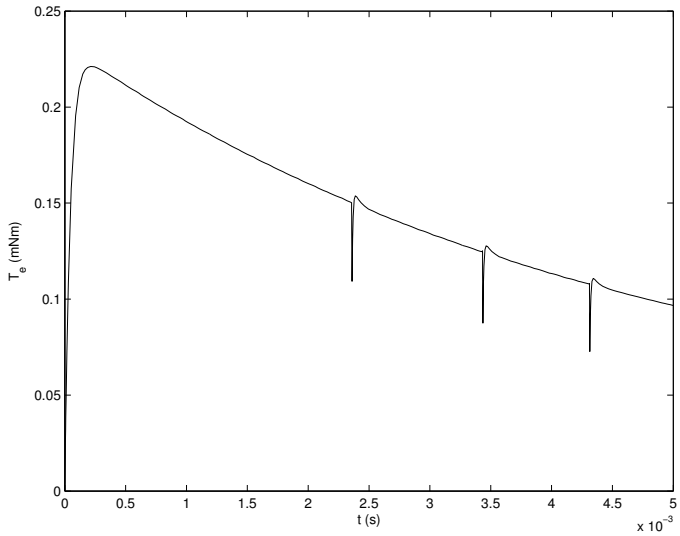

Figure 5.36: Electrical torque in variable dc-link voltage speed control at no load ($\alpha_\omega = 0.01\alpha_e$)

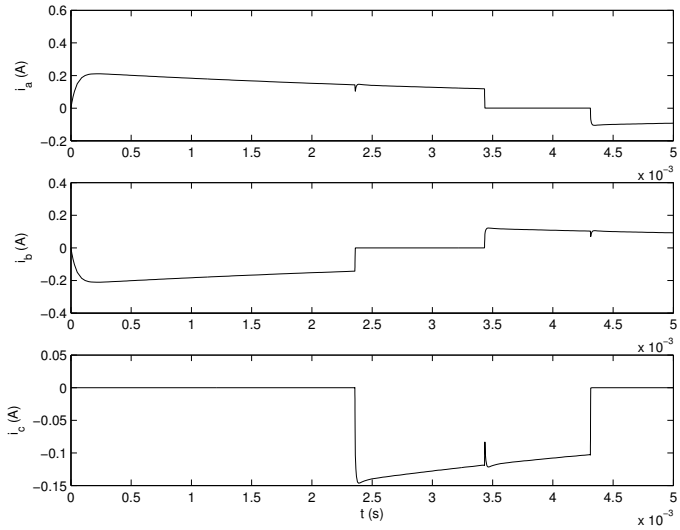

Figure 5.37: Phase currents in variable dc-link voltage speed control at no load ($\alpha_\omega = 0.01\alpha_e$)

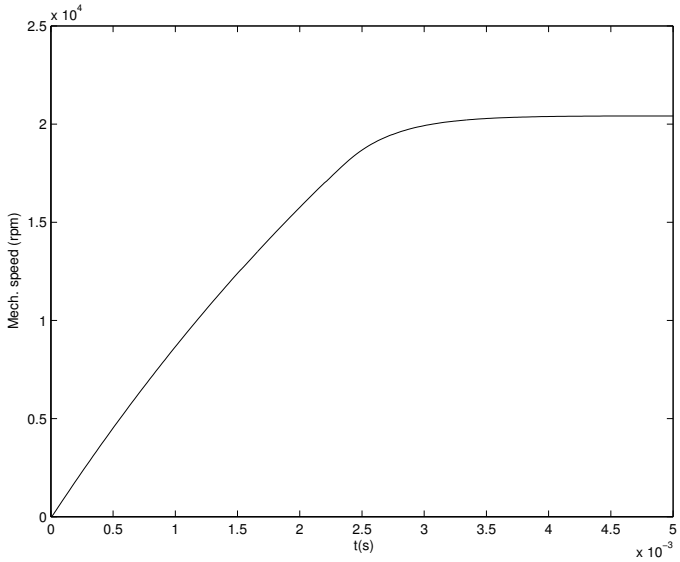

Figure 5.38: Rotor speed in variable dc-link voltage speed control at no load ($\alpha_\omega = 0.1\alpha_e$)

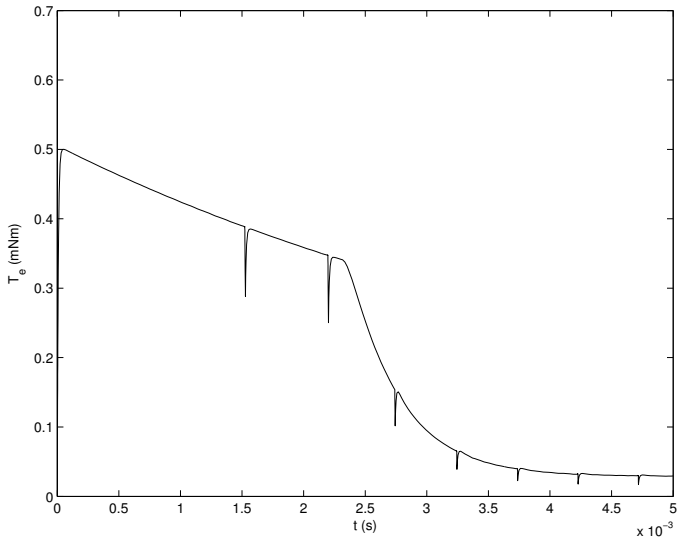

Figure 5.39: Electrical torque in variable dc-link voltage speed control at no load ($\alpha_\omega = 0.1\alpha_e$)

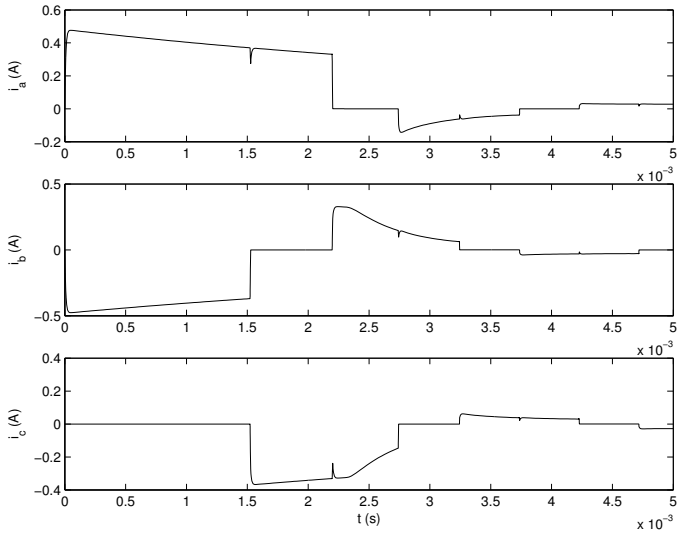

Figure 5.40: Phase currents in variable dc-link voltage speed control at no load ($\alpha_\omega = 0.1\alpha_e$)

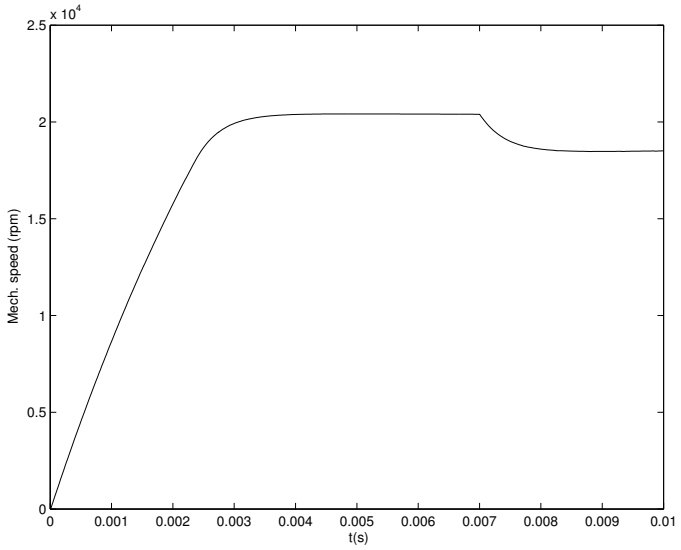

Figure 5.41: Rotor speed in variable dc-link voltage speed control at maximum load step ($\alpha_\omega = 0.1\alpha_e$)

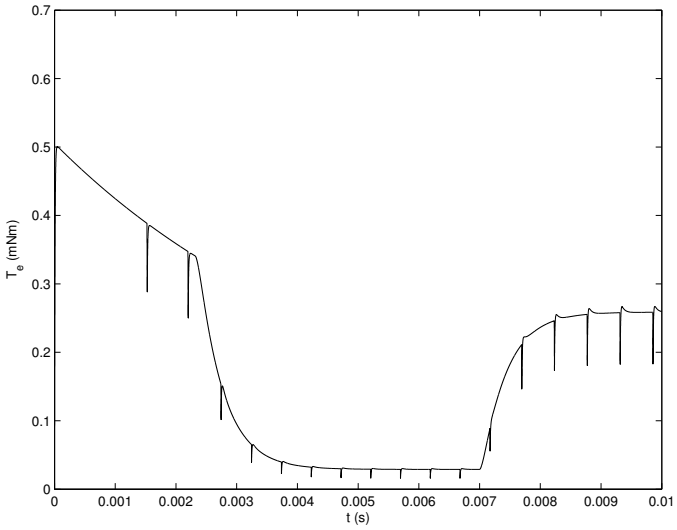

Figure 5.42: Electrical torque in variable dc-link voltage speed control at maximum load step ($\alpha_\omega = 0.1\alpha_e$)

5.3.3 Position Control

The position controller is the same as the one used in the pwm control, and the reference angle is again 3600°. Figure 5.43 shows the whole system.

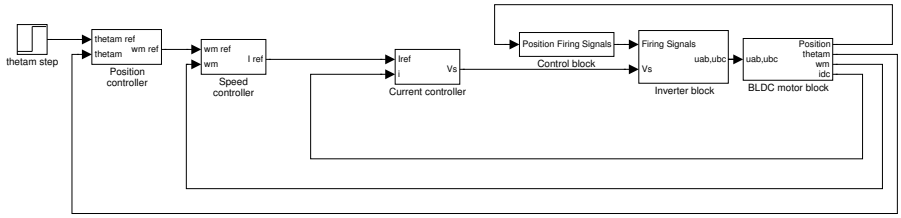

Figure 5.43: Varible dc-link voltage position control system

The controller parameters are the same as before and figures 5.44 and 5.45 show the rotor angle at no load and at maximum load. The two curves are identical, and the control error is negligible as in the pwm control part. The same applies here as with the pwm control; if an overshoot occurs, there is no way to correct the error, so a compromise must be made between fast response and accuracy.

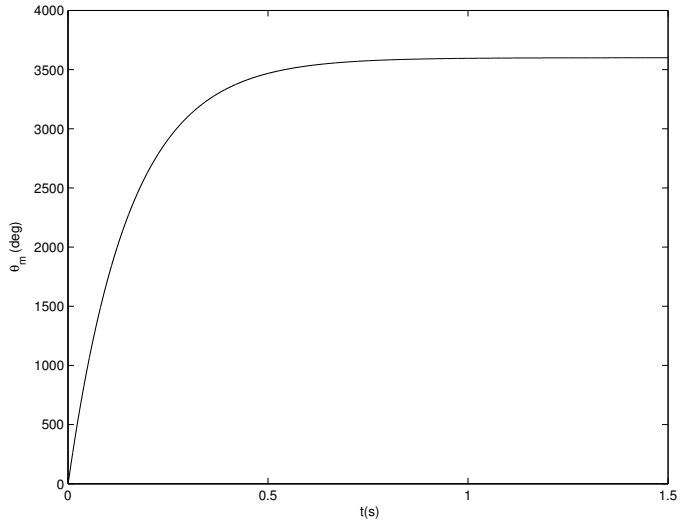

Figure 5.44: Rotor angle in variable dc-link voltage position control at no load

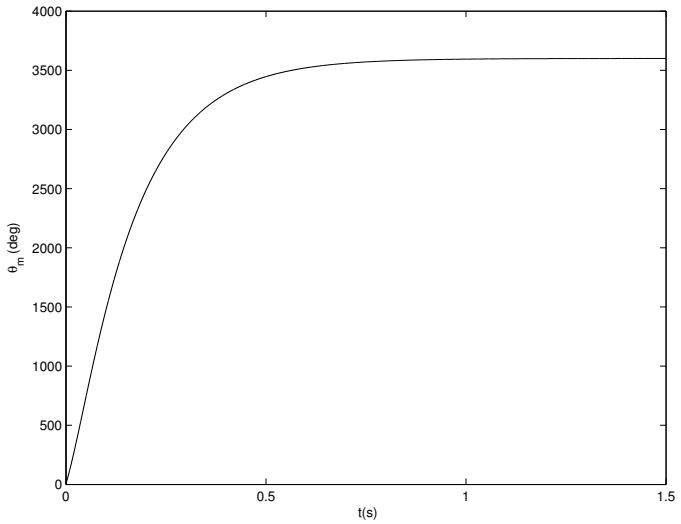

Figure 5.45: Rotor angle in variable dc-link voltage position control at maximum load

5.4 Frequency Analysis

5.4.1 Uncontrolled motor

The frequency spectrum of current is an important factor in all electric systems. Undesirable frequency content can create disturbances in other equipment and losses in the motor. The current drawn by bldc motors is not a perfect dc current. The current has narrow notches which are the cause of torque ripples. There are six commutations per each electrical cycle so it is easy to derive that the frequency of the commutation ripples is

$$f_{com} = \frac{p}{2} \cdot \frac{n}{10} \tag{5.7}$$

where p is the number of poles and n is the rotor speed in rpm.

Figure 5.46 shows a zoomed view of the electrical torque at no load speed (47,000 rpm approx.). The notches in the torque are narrow and their depth is about 45% of the peak torque. The relative depth of the notches becomes less as the load increases. Figure 5.47 shows that at maximum load the notches reach about 30% of the peak torque.

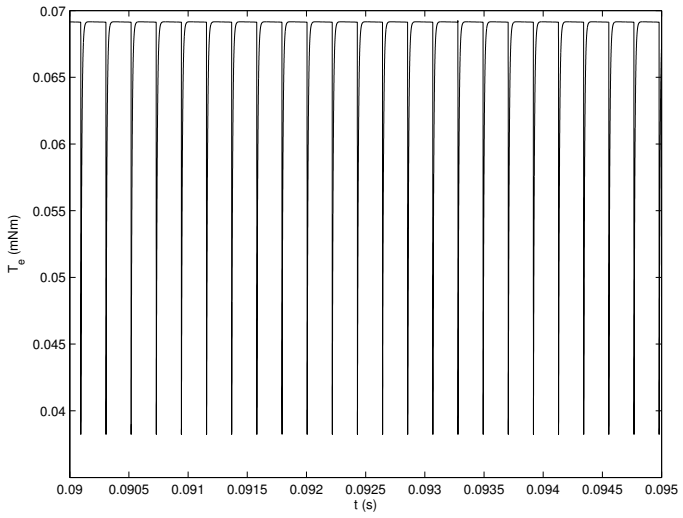

Figure 5.46: Zoomed view of the electrical torque at no load speed

The power spectrum of the dc-link current at no load speed is shown in figure 5.48. The fundamental frequency is around 4.7 kHz which agrees with the value given by equation 5.7. The harmonics of the fundamental frequency are quite strong as the figure shows.

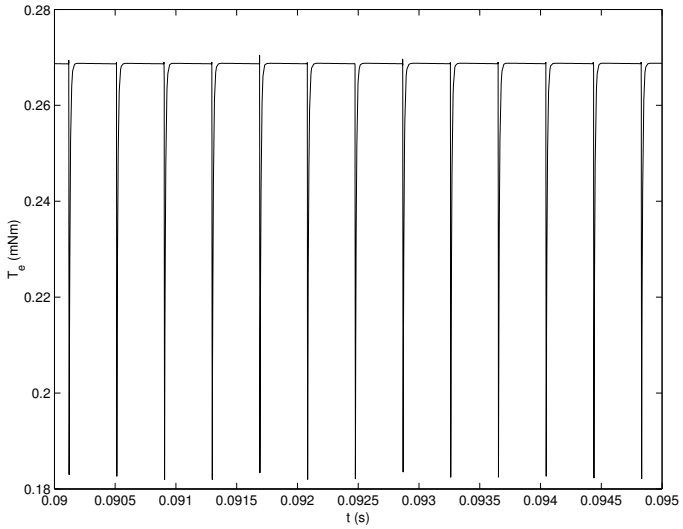

Figure 5.47: Zoomed view of the electrical torque at maximum load

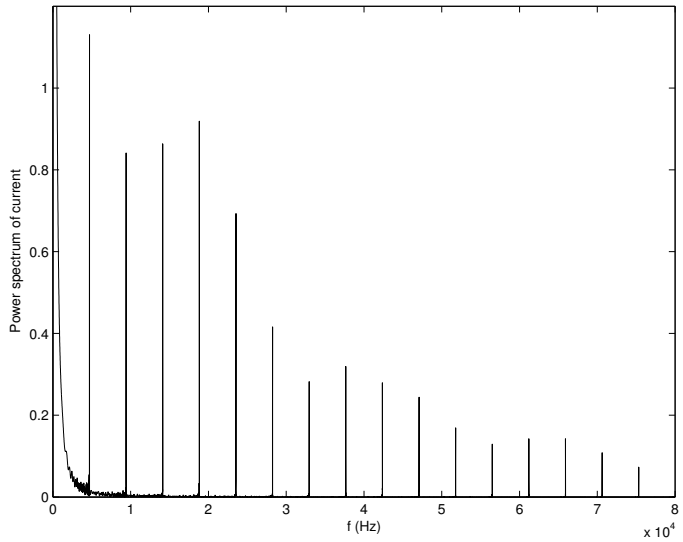

Figure 5.48: Power spectrum of the dc-link current at no-load speed

5.4.2 Hysteresis control

Figures 5.49 and 5.50 show the dc-link current power spectrum at no load and at maximum load respectively, while the speed is held constant at 20,000 rpm. Figure 5.49 shows that the fundamental frequency at no load is roughly 2 kHz. At maximum load the fundamental frequency becomes almost 4 kHz as shown in figure 5.50. The commutation notches are no longer the main source of harmonics. The switching frequency of hysteresis controller dominates the frequency spectrum.

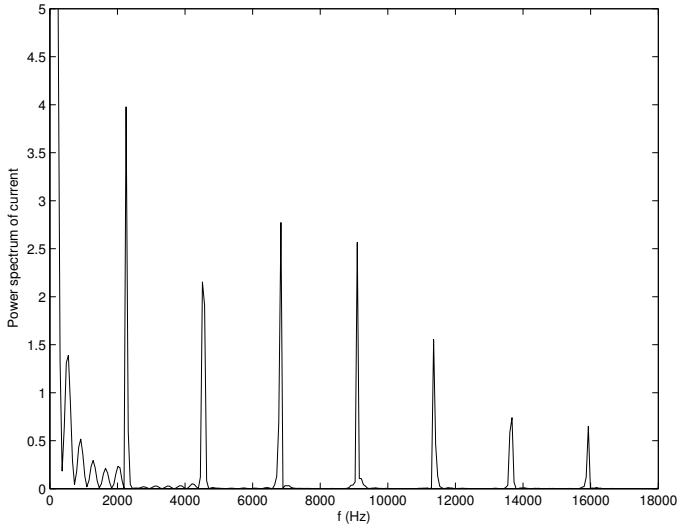

Figure 5.49: Power spectrum of the dc-link current in hysteresis speed control at no load

The power spectrum shown in the figures shows clearly how the switching frequency varies with varying load. This is the main drawback of hysteresis control because it makes it difficult to filter out unwanted harmonics.

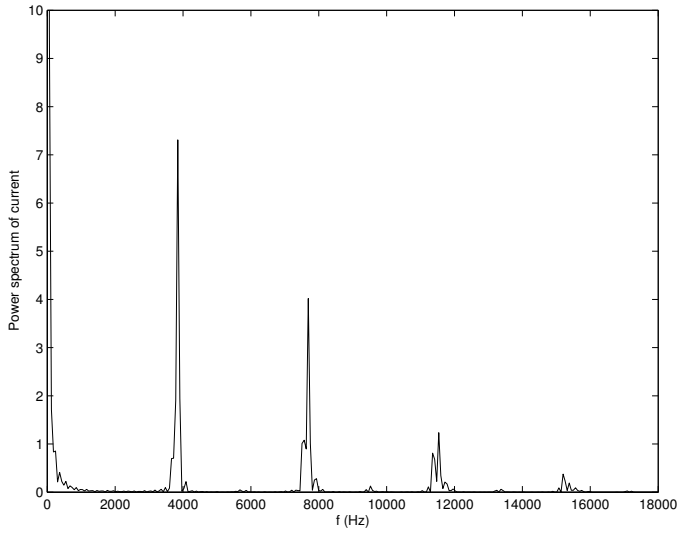

Figure 5.50: Power spectrum of the dc-link current in hysteresis speed control at maximum load

5.4.3 PWM

Figures 5.51 and 5.52 show the same power spectrum as the two previous figures now using pwm control. The conditions are the same; no load, maximum load and constant speed. The figures show that the frequency content is independent of load and that the fundamental frequency is the 50 kHz pwm frequency. The other peaks are harmonics of that frequency. The fixed frequency of the pwm technique is what makes it more popular than the hysteresis band technique, as filtering becomes much easier.

5.4.4 Variable DC-Link Voltage

The varible dc-link voltage technique does not involve any current chopping and it therefore only contains harmonics that depend directly on the rotor speed. The current spectrum will look like the one in figure 5.48 with a fundamental frequency defined by equation 5.7.

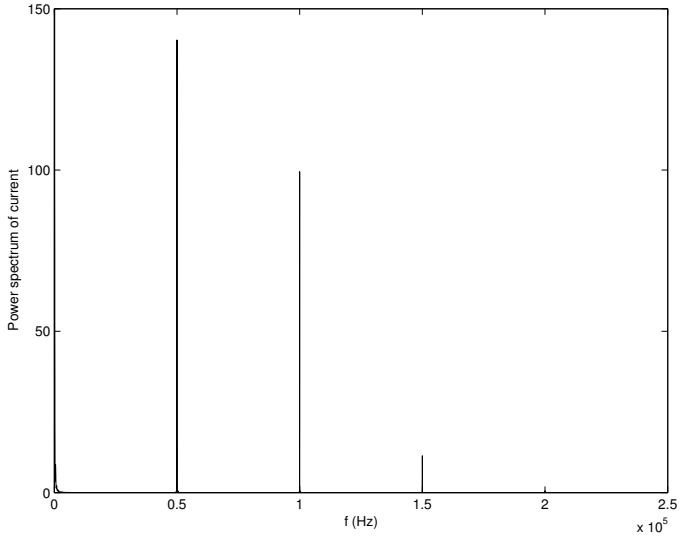

Figure 5.51: Power spectrum of the dc-link current in pwm speed control at no load

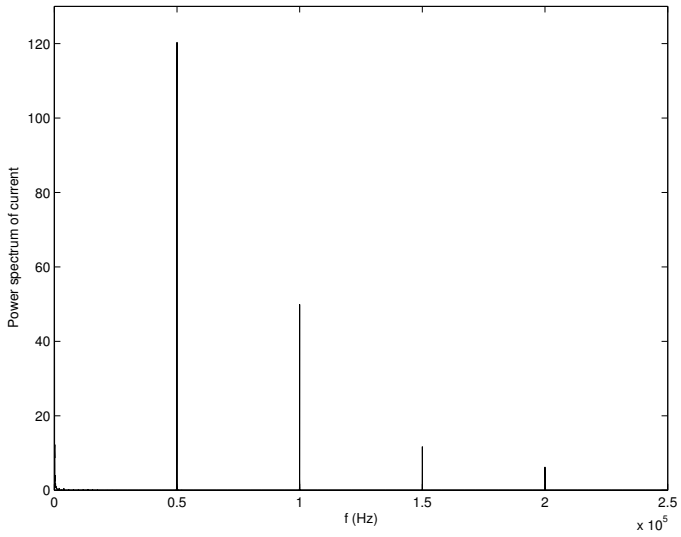

Figure 5.52: Power spectrum of the dc-link current in pwm speed control at maximum load

Chapter 6

Turn-ON Delay and Losses

The inverter used in the simulations has so far been modelled as an ideal device containing very fast lossless switches. In practice, things like resistive losses and turn-off time must be taken into account. Semiconductor switches have some resistance even when they are fully *on* which causes voltage drop and heating. Even more power is dissipated during very short intervals when the switch is going from non-conductive state to conductive state and vice versa. It is known that semiconductor switches take more time to turn off than to turn on [8]. In cases where the turn-on signal is being transferred from one switch to another switch in the same leg, some measures must be taken to avoid shoot-through (short circuit). This chapter briefly discusses the effects of turn-on delay and on-state losses.

6.1 Turn-ON Delay

As mentioned above, turn-on delay of switches is necessary to prevent shoot-through and to ensure smooth commutation. The turn-off time is specified in the switches' datasheets and a turn-on delay should be chosen accordingly. The turn-on delay should be kept as short as possible as it can have negative side effects as will be shown here. Figure 6.1 shows the three phase-currents when a turn-on delay is applied at 0.03 s. Load torque is zero and the delay time is about 1 ms which should be enough for most switches. The figure shows that the commutation notches become deeper when the delay is applied. This results in greater torque ripples as shown in figure 6.2. The ripples appear, of course, also in the dc-link current and increase the magnitude of the switching frequency component in the current power spectrum.

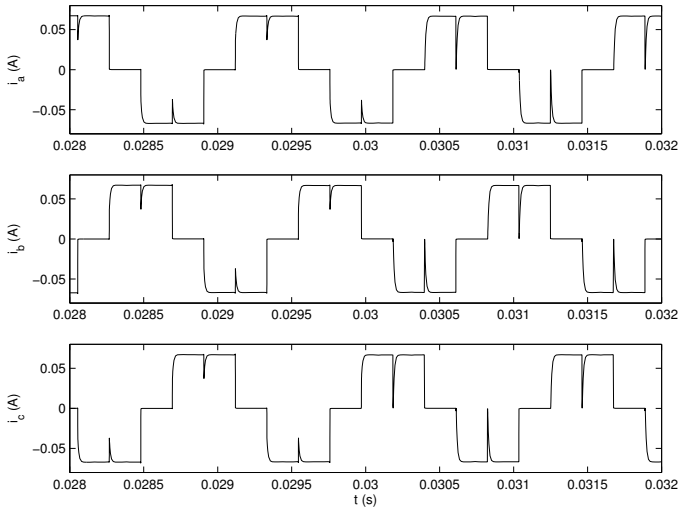

Figure 6.1: Phase currents. A 1 ms turn-on delay is applied at 0.03 s

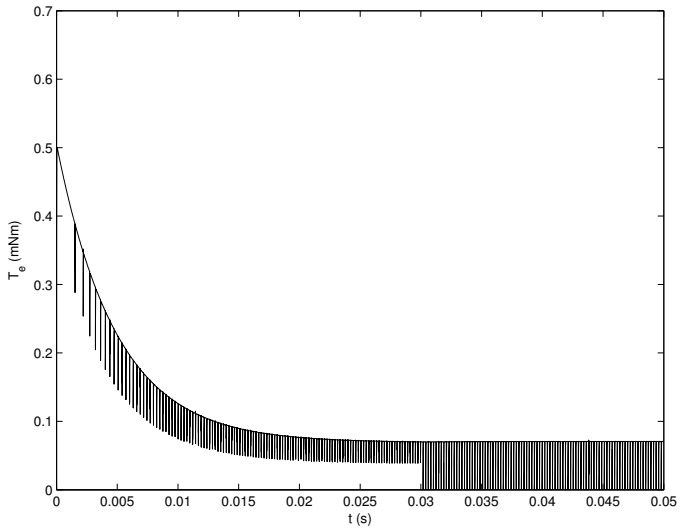

Figure 6.2: Electrial torque. 1 ms turn-on delay is applied at 0.03 s

6.2 ON-state Losses

Figure 6.3 shows the rotor speed when maximum load step is applied at 0.05 s. The on-resistance of each switch is 2 Ω giving a total of 4 Ω. Comparing figures 6.3 and 6.4 with figures 4.16 and 4.17 (pages 28 and 29) reveals that the switch resistance causes both lower speed and lower torque. This is not surprising since the motor terminal voltage becomes lower. Figure 6.5 shows the power dissipated in the switches.

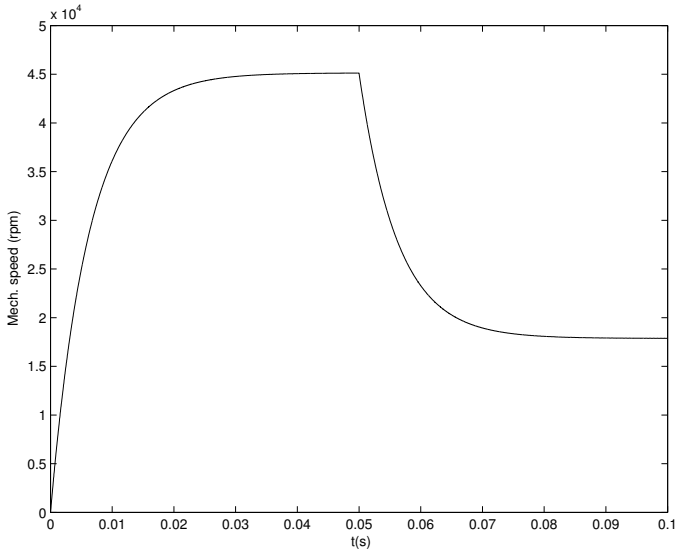

Figure 6.3: Rotor speed when on-state resistance of switches is 2 Ω

PWM and hysteresis control introduce more losses since they involve high frequent switching. The switching frequency in hysteresis control can vary alot but if load torque is constant, the frequency can be tuned by selecting a suitable tolerance band. The pwm switching frequency can however be chosen explicitly. Too high a frequency causes excessive losses but too low a frequency will make the motor currents become a series of high pulses instead of continuous varying current. A compromise must be made and the optimal frequency will depend on the characteristics of the motor and the switches [8].

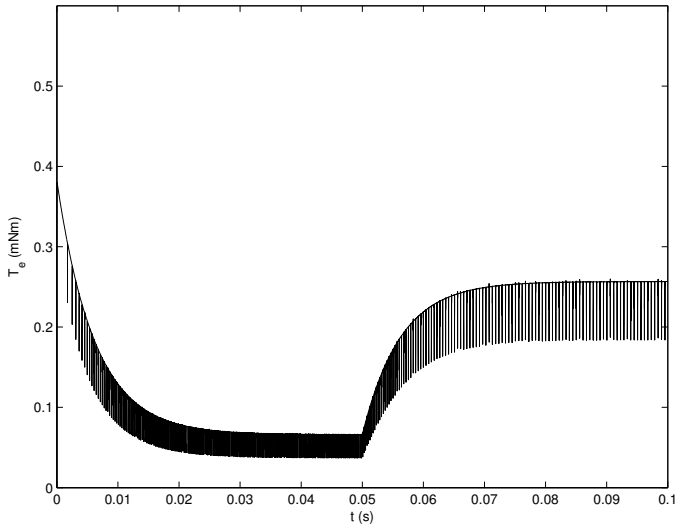

Figure 6.4: Electrical torque when on-state resistance of switches is 2 Ω

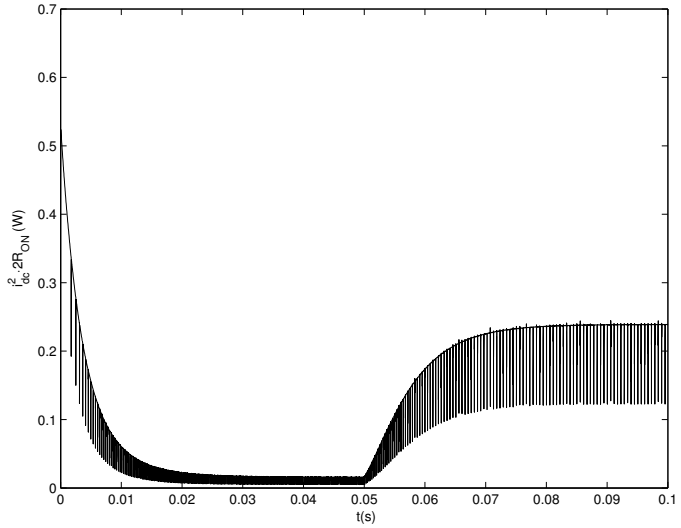

Figure 6.5: Power dissipation in switches when on-state resistance is 2 Ω

Chapter 7

Conclusions

7.1 Summary

In this thesis, a Matlab®/Simulink® model of a three phase star-connected bldc motor was developed. The main part of the work was involved in the development of the six step inverter and its interaction with the motor. The aim was to make a model that would be simple, accurate, easy to modify and fast running. It is believed that these goals have been reached. Parameters of a real bldc motor were used and it was verified that the model performed according to the information given in the motor's datasheet. A simple model of a dc motor was also implemented to show the similarity of the two motors.

Torque-, speed- and position control was implemented using three different control strategies: hysteresis band control, pwm control and variable dc-link voltage control. All the control methods performed well but each has its drawback.

The uncontrolled switching frequencies of the hysteresis band technique may be unacceptable in many cases and swithing losses may be a problem if the hysteresis band is very narrow. Analysis in the frequency domain showed clearly that the frequency content of the dc-link current is highly dependent on the applied load. This makes filtering difficult so the hysteresis band technique may be suitable only in applications where load variations are small.

The pwm control worked very well and would in most cases be a better alternative than hysteresis band control. There was, however, some steady state speed-control error but the cause of it was not investigated due to time limitations. The position controller performed very well with practically zero error. Because of the fixed switching frequency, the frequency content of the dc-link current is independent of load variations which makes filtering of

unwanted harmonics relatively easy. A 50 kHz switching frequency was used which is quite high. Such a high frequency was chosen because the motor can operate at very high speed. Such high frequency may cause excessive switching losses but the magnitude of the losses was not investigated here.

The variable dc-link voltage technique is the only technique that does not cause high frequency disturbances, at least if it is assumed that the variable voltage source is ideal. Its performance was similar to the pwm method but it produced much smoother torque due to the absence of high frequent switching. In the frequency domain, the variable dc-link voltage technique contains only harmonics caused by the current commutation. These frequencies are proportional to the rotor speed and can easily be calculated.

Finally, losses and commutation delay were investigated. Only on-state losses were considered and simulations showed that even though currents and on-resistance are small, its effects are clearly noticable. The side-effects of a commutation delay showed that the delay should be kept as short as possible beacause the delay increases the infamous torque ripples of the bldc motor.

7.2 Further Work

One of the advantages of the bldc motor model presented here is that it is not overly complicated. Improvements and additions are therefore very easy to make. One additional feature could be to extend the motor operaton to four quadrants. This is easy to implement but it will surely cause longer simulation time. The inverter now supports both hard and soft chopping operation, but only soft chopping was used in the simulations. The two chopping methods could be compared and their effects on torque ripple investigated. Other control methods could be tested on the model. This might involve using one current controller for each phase. Sensorless control techniques could also be implemented. This could involve a special method to start the motor until the speed becomes high enough for detection of back-emf. The shape of the back-emf could also be changed to a non-ideal waveform with smoother edges. Finally, a logical next step would be to try the different control strategies on a real bldc motor

Bibliography

[1] Daniel Hansson. Study and test of a bldc motor drive systems function and operation fora pump application. Master's thesis, Institutionen för Elteknik, Chalmers Tekniska Högskola, 2004.

[2] Padmaraja Yedamale. *Brushless DC (BLDC) Motor Fundamentals*. Microchip Technology Inc., 2003.

[3] Juan W. Dixon and Iván Leal. Current control strategy for brushless dc motors based on a common dc signal. *IEEE Transactions on Power Electronics*, 17(2), March 2002.

[4] Saurabh Gupta. Control of a brushless dc machine as a part of a free piston energy converter for a hybrid electric vehicle. Master's thesis, Department of Electric Power Engineering, Chalmers University of Technology, 2003.

[5] P.C. Sen. *Principles of Electric Machines and Power Electronics*. John Wiley & Sons, 1997.

[6] Lennart Harnefors. *Control of Variable-Speed Drives*. Mälardalen University, 2002.

[7] Texas Instruments Incorporated. *DSP Solutions for BLDC Motors*, 1997.

[8] Ward Brown. *Brushless DC Motor Control Made Easy*. Microchip Technology Inc., 2002.

[9] P C K Luk and C K Lee. Efficient modelling for a brushless dc motor drive. In *Industrial Electronics, Control and Instrumentation*, 1994.

[10] Maxon Precision Motors Inc., `http://www.maxonmotor.com/docsx/Download/catalog_2005/Pdf/05_150_e.pdf`. *EC 6 $\oslash$6mm, brushless, 1.2 Watt*, 2005.

[11] K.S. Low M.F. Rahman and K.W. Lim. Approaches to the control of torque and current in a brushless dc drive.

[12] Maxon Precision Motors Inc., `http://maxonmotor.com/docsx/Download/catalog_2005/Pdf/05_Technik_kurzun%d_buendig_mmc_32_33_e.pdf`. *Maxon Motor Control, Technology - short and to the point.*

[13] Kyeong-Hwa Kim and Myung-Joong Youn. Performance comparison of pwm inverter and varible dc link inverter schemes for high-speed sensorless control of bldc motor. *Electronics Letters*, 38(21):1294–1295, October 2002.